G.I.S. MAPPING OF UPLIFTED COASTAL TERRACES USING DIGITAL TERRAIN MODELS, NICOYA PENINSULA, COSTA RICA

A Thesis

Presented to the

Faculty of

California State Polytechnic University, Pomona

In Partial Fulfillment

Of the Requirements for the Degree

Master of Science

In

Geological Sciences

By

Melissa V. Robinson

2016

SIGNATURE PAGE

THESIS:	G.I.S. MAPPING OF UPLIFTED COASTAL TERRACES USING DIGITAL TERRAIN MODELS, NICOYA PENINSULA, COSTA RICA
AUTHOR:	Melissa V. Robinson
DATE SUBMITTED:	Spring 2016
	Geological Sciences Department

Dr. Jeffrey Marshall
Thesis Committee Chair
Geological Sciences _____

Dr. Jonathan Nourse
Geological Sciences _____

Dr. Stephen Osborn
Geological Sciences _____

Dr. Bryan Murray
Geological Sciences _____

ACKNOWLEDGEMENTS

I would like to thank my family for all of their support and bribery, Rico and Jave, Dr. Marshall for his unfailing knowledge of relevant papers and years of research in Costa Rica, and all of the friends I've found in the Cal Poly Geology Department.

ABSTRACT

Digital Terrain Models (DTMs) manipulate elevation data and display it spatially. This project modifies an existing method used to identify and extract low-relief landscape surfaces (e.g., marine terraces) using DTMs constructed in ArcGIS. The terrace extraction method uses slope, relief, and elevation DTMs to select cells that have values typical of gently sloping marine terraces, while avoiding false positive values that may be associated with other surfaces, like ridge tops and stream beds. The extraction procedure was modified to work with a smaller cell size, and was calibrated to locate uplifted marine terraces along the coastlines of the Nicoya Peninsula, Costa Rica. Five previously mapped field areas were used as source data to determine the best combination of input values for the Nicoya Peninsula. Based on iterative testing, the optimum input values were determined (slope $\leq 15^{\circ}$, relief ≤ 15m within a radius of 87.5m, elevation ≥ 0m) and the terrace extraction procedure was extrapolated across the entire Nicoya Peninsula. Elevation values were extracted and segmented two different ways: first according to offshore boundaries between the EPR, CNS-1, and CNS-2 crustal types, and then according to major geomorphic boundaries seen on the peninsula. Terrace elevations were combined with isotopic age data and correlated with sea level high stands to calculate uplift rates. A subtle shift in uplift rates (~0-0.5 m/ka to ~0.2-0.7 m/ka) can be seen at the EPR/CNS-1 boundary. A large jump in uplift rates (up to 1.5-2.5m/ka) occurs at the CNS-1/CNS-2 boundary. Further field work is necessary to identify unknown surfaces and verify uplift trends.

TABLE OF CONTENTS

LIST OF TABLES

LIST OF FIGURES

INTRODUCTION

This thesis presents the results of a two-part investigation of uplifted Quaternary marine terraces located on the Nicoya Peninsula, Costa Rica. The first part of the investigation involves the testing of a methodology – using the geospatial analysis of topographic data to determine the locations and characteristics of unmapped marine terraces in a region with site-specific field data. The second part of the investigation makes use of the information acquired in Part 1 to determine uplift rates for the late-Pleistocene marine terraces along the Nicoya Peninsula and to interpret those uplift rates to further our understanding of the subsurface structure of the offshore subduction zone.

TERRACE MORPHOLOGY

Coastal geomorphology describes three different types of coastal beach environments: rocky, sandy and coral (Anderson and Anderson, 2010). In this study, the rocky beach morphology [Figure 1] best fits the features seen along the Nicoya coastline. A rocky beach is formed when a gently sloping coastal platform meets a rocky cliff or deposit on the shore and wave erosion drives the sea cliff landward (Bradley and Griggs, 1976). The platform is referred to as a wave-cut platform because its shape is dependent on the waves that move over it and erode it. During periods of rising sea level, wave erosion pushes the sea cliff landward, expanding the width of the wave-cut platform. When sea level falls, the platform is abandoned and terrace deposits made up of beach, fluvial, and colluvial sediments subsequently cover the wave-cut platform. In tectonically active regions, these abandoned wave-cut platforms can be uplifted beyond

the reach of wave erosion and preserved as marine terraces before sea level rises again to a new sea level high stand (LaJoie, 1986; Anderson et al., 1999). During the Quateranry, global sea level has fluctuated dramatically between multiple high stands and low stands related to repeated glacial and interglacial cycles. Quaternary marine terraces are useful geomorphic markers because they denote horizontal lines with a known initial elevation derived from eustatic sea level history. The ocean erodes the base of the previous coastal deposit, or cliffs, creating a line that marks the mean sea level at that period of time. This line that connects the wave-cut platform to the corresponding sea cliff is referred to as the wave-cut angle [Figure 1], or the inner edge. By documenting the inner edge elevations along a stretch of coastline, one reveals a pattern of relative land level change since the time of formation of the marine terrace. If the terrace is dated, a long-term mean uplift rate can be found (LaJoie, 1986; Anderson et al., 1999). A similar feature, referred to as the back-edge of a terrace marks the line seen in the field, where the terrace tread (top of terrace sediment deposits) meets the corresponding sea cliff. Both the field data and the terrace extraction procedure in this paper identify the back-edge of the terrace rather than the true inner-edge of the wave-cut platform, which lies at several meters depth beneath the terrace deposits.

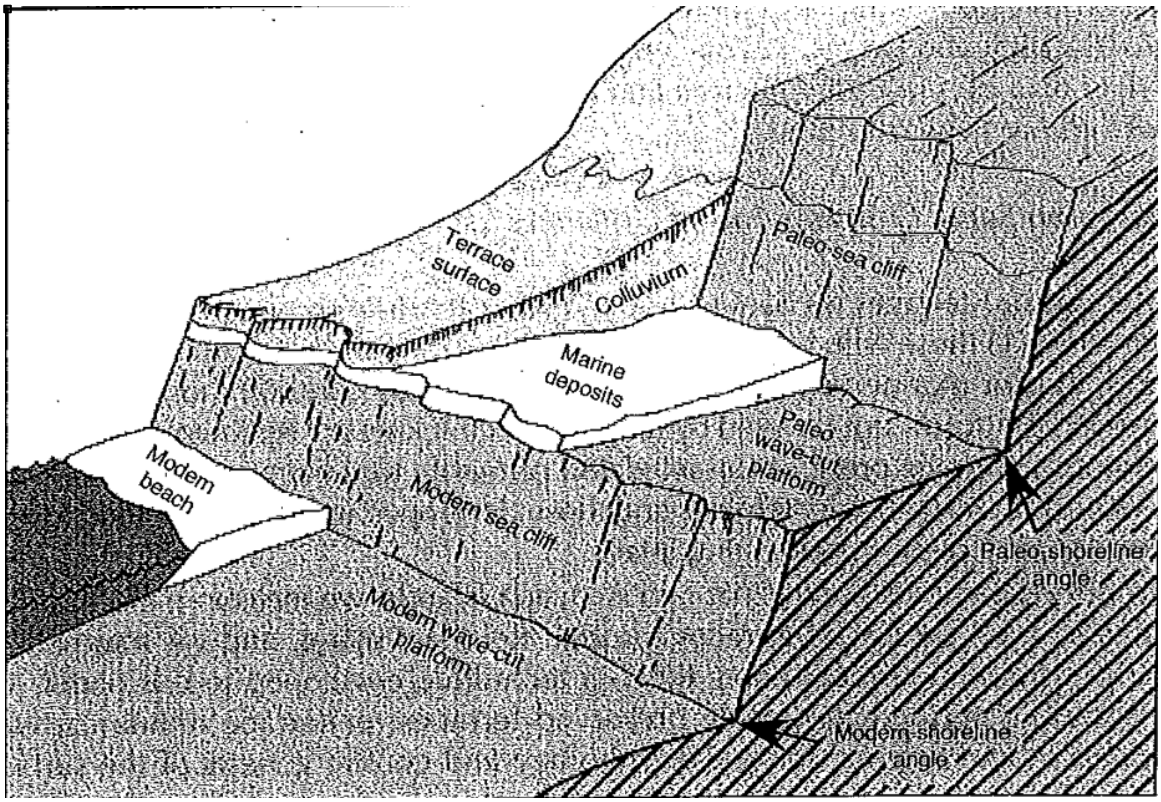

Figure 1: Schematic of uplifted marine terrace geomorphology (Scott and Pinter, 2003).

TERRACES ON THE NICOYA PENINSULA

Location

The Nicoya Peninsula [Figure 2] is a prominent feature found along the west coast of Costa Rica. Separated from the Costa Rica mainland by the Gulf of Nicoya and the Tempisque River basin, the Nicoya Peninsula makes up a large portion (4800 km^2) of the Chorotega forearc province of southern Central America (Marshall, 2007). Coastal topography varies greatly on each side of the peninsula. The Pacific coastline features many small bays and sandy beaches bounded by rocky headlands that are indicative of active uplift, while the gulf coast of the peninsula features marshy mangrove estuaries that grade into a low-relief alluvial plain indicative of subsidence (Marshall, 2007).

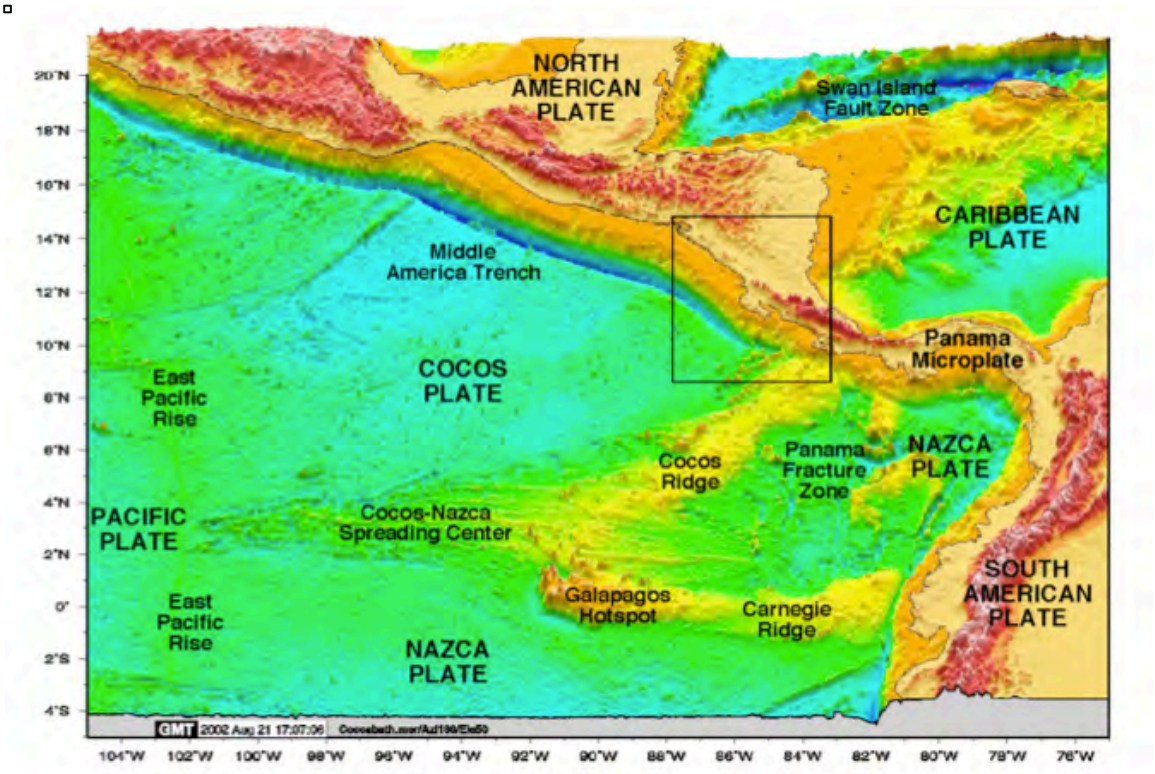

Figure 2: Tectonic map of Central America and adjacent seafloor consisting of the Cocos, Nazca, and Caribbean plates (after IFM-GEOMAR). The Middle America Trench marks the convergent margin where the Cocos plate subducts in a northeast direction beneath the Caribbean Plate at 8-10 cm/yr. This image shows the structure of the Cocos Plate, especially the boundary between smooth seafloor formed at the East Pacific Rise and rough seafloor formed at the Cocos-Nazca spreading center. This boundary intersects the margin offshore of the Nicoya Peninsula (center of black box).

Tectonic Setting

The Nicoya Peninsula [Figure 2, Figure 3] is located on the northwestern coast of Costa Rica and lies alongside the Middle America Trench. The Middle America Trench marks the active subduction zone where the Cocos Plate subducts beneath the Caribbean Plate [Figure 2] at a rate of 8.3±0.2 cm/year in a northeast direction (DeMets et al., 2010).

The Cocos Plate has a complex tectonic history (e.g., Hey, 1977; Barckhausen et al., 2001) that resulted in segmentation of the plate into three types of oceanic crust [Figure 3, Figure 4] which are defined as follows (Barckhausen et al., 2001):

1) EPR – The EPR oceanic crust is named as such because it originates at the East Pacific Rise. It is a smooth oceanic seafloor and is the oldest (>23 Ma), coldest and densest of the three types of crust.
2) CNS-1 – The CNS-1 oceanic crust originated at the Cocos-Nazca Spreading Center. While also a smooth oceanic crust, it is younger (23-19 Ma), thermally warmer, and more buoyant than its EPR counterpart.
3) CNS-2 - The CNS-2 oceanic crust also originates at the Cocos-Nazca Spreading Center, but is younger (<19 Ma) and rougher than CNS-1, containing abundant seamounts produced by hot spot volcanism at the Galapagos Hot Spot.

The boundary between the EPR and CNS-1 crust is a fracture trace that marks the migration of a triple point boundary around 23 Ma [Figure 4]. The boundary between CNS-1 and CNS-2 is caused by a ridge jump of the triple junction that occurred around 19 Ma. (Barckhausen et al., 2001).

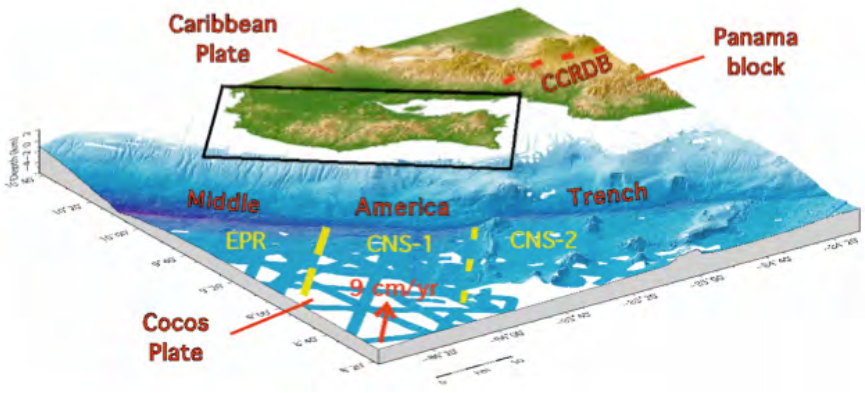

Figure 3**:** Digital Elevation Model of Costa Rica (NASA-SRTM) linked to offshore bathymetry (IFM-GEOMAR). Two segment boundaries on the subducting Cocos Plate (Barckhausen et al., 2001) intersect the Middle America Trench offshore of the Nicoya Peninsula: 1) a morphologic break between the smooth and rough seafloor (short dashed line) and 2) a fracture zone trace (long dashed line) that separates crust formed at the East Pacific Rise (EPR) from crust formed at the Cocos Nazca Spreading Center (CNS-1, CNS-2). Marine terrace study sites (Marshall et al., 2012) are located along the seaward coastline of the Nicoya Peninsula (black box).

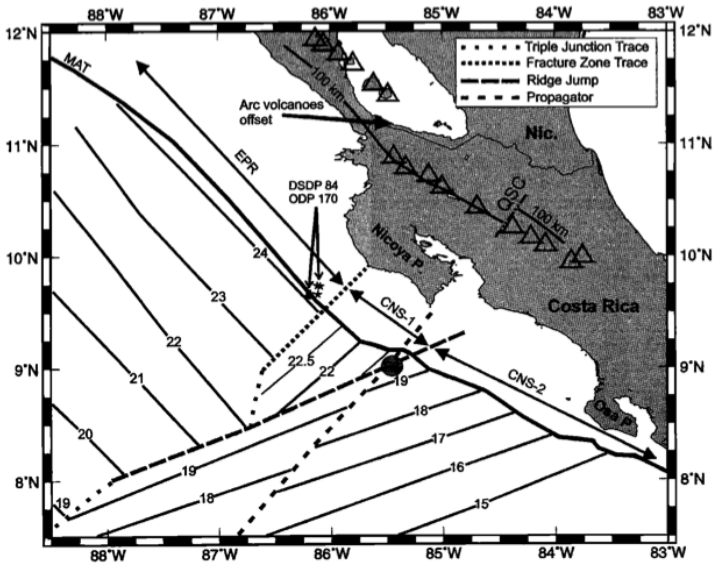

Figure 4: Tectonic segments of Cocos Plate seafloor off the coast of the Nicoya Peninsula. Three distinct seafloor domains (EPR, CNS-1, CNS-2) are subducting along the Middle America Trench (MAT) offshore Costa Rica. Lines with numbers depict seafloor age based on magnetic anomalies (from Barckhausen et al., 2001).

Regional Geology

The Nicoya Peninsula consists of an uplifted portion of Caribbean plate seafloor on the landward side of the Middle America Trench (Lundberg, 1982). The basement geology is an ophiolite sequence called the Nicoya Complex (Dengo, 1962). The Nicoya Complex has proven to be more complicated, however, than a textbook ophiolite sequence and is often divided into two major units (Lundberg, 1982). The lower unit is predominantly basaltic; a massive or pillow basalt unit that has little or no sediment within the basalt layers. The upper unit of the Nicoya Complex is more heterogeneous and may represent an early volcanic arc. This unit contains pillow basalts, volcanic agglomerates, and tuffaceous sediment interspersed with chert and siliceous limestone (Lundberg, 1982). Radiometric dating of the two units of the Nicoya Complex show that both units are similar in age (80-90 Ma) (Sinton et. al., 1997).

The sedimentary units above the Nicoya Complex consist of a predominantly pelagic depositional environment within the older units and then the units shallow upwardly to younger shallow water deposits (Baumgartner et al., 1984). These sediments include limestone, mudstone, and conglomerate units, as well as volcanic ash layers. Cenozoic shallow water deposits (e.g. reef limestones) indicate that much of the area was uplifted by the Eocene (Lundberg 1982). Continued uplift though the present resulted in the deposition of Plio-Pleistocene coastal sandstones and conglomerates, as well as the formation of Pleistocene through Holocene terraces (e.g., Hare and Gardner, 1985; Marshall and Anderson, 1995; Marshall et al., 2008, 2010, 2012).

This study looks at the western coast of the Nicoya Peninsula, where the underlying bedrock is a basaltic unit of the Nicoya Complex. The continuity of this

basaltic unit along most of the coastline [Figure 5], except for the region between Nosara and Carrillo (made up of sedimentary units) allows for the assumption of relatively equivalent values for erosion and rock strength along the peninsula.

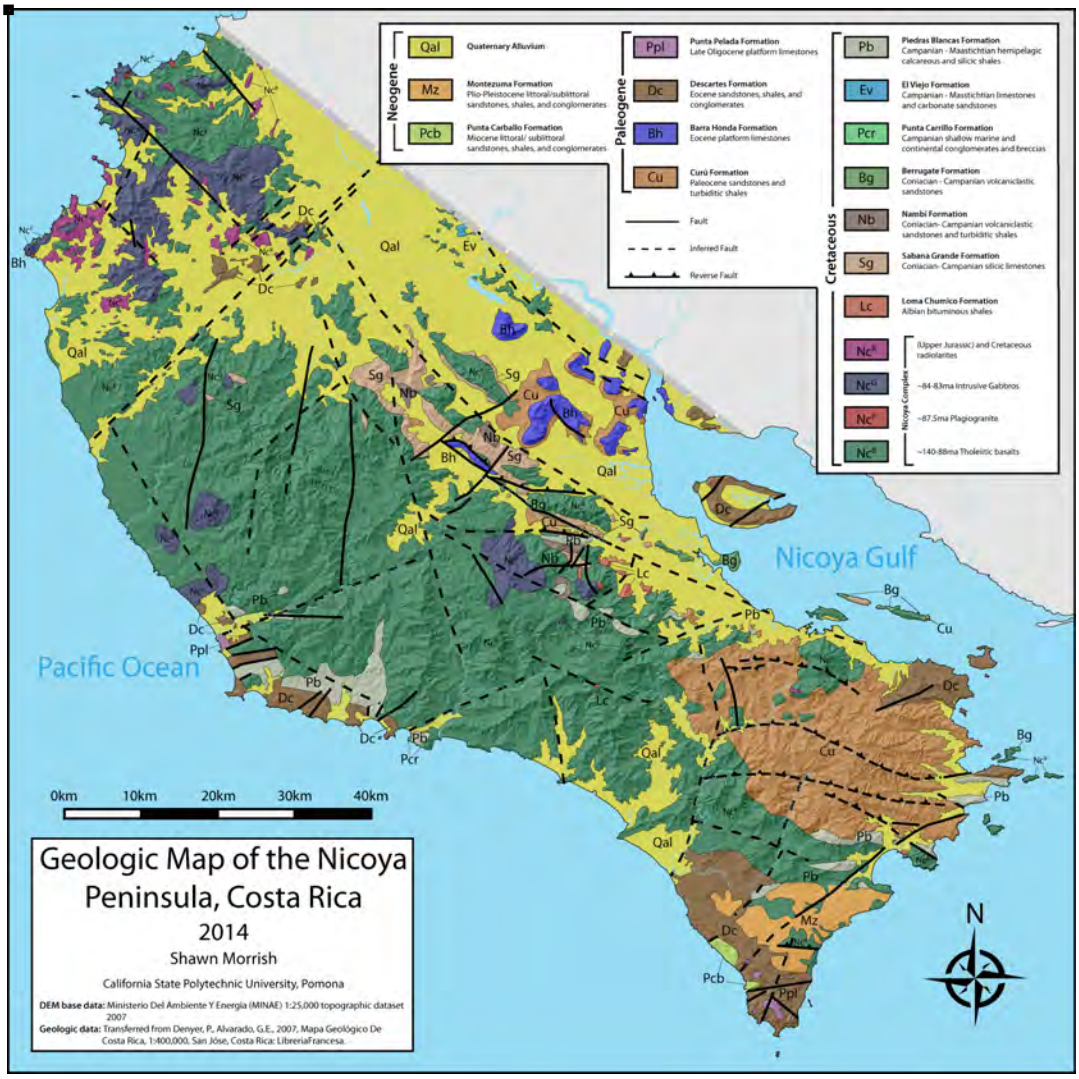

Figure 5: Geologic Map of the Nicoya Peninsula (Morrish, 2015; after Denyer and Alvarado, 2007).

Tectonic Geomorphology

Due to its close proximity to the subduction zone, the coastline of the Nicoya Peninsula is particularly sensitive to vertical crustal motions related to under-thrusting of the Cocos plate seafloor (Marshall, 2007). Differences in plate roughness, thermal structure, and fluid flow between the three types of subducting crust (EPR, CNS-1, CNS-2) result in strong variations in plate margin seismicity and forearc deformation along the Nicoya Peninsula (e.g., Marshall and Anderson, 1995; Newman et al., 2002; Marshall et al., 2012).

This project focuses on upper-plate uplift as expressed by late Quaternary marine terraces overlying the EPR to CNS-1 and CNS-1 to CNS-2 crustal boundaries on the subducting Cocos Plate [Figure 3]. The position of these boundaries on the subducting plate [Figure 4] was first mapped in detail using magnetic anomalies (Barckhausen et al., 2001). This anomaly map reveals both the location of the triple junction trace (EPR-CNS-1 boundary) formed at the intersection of the East Pacific Rise and Cocos-Naza Spreading Center (Hey, 1977), as well as a later ridge jump between the CNS-1 and CNS-2 crusts (Barckhausen et al., 2001).

Prior geomorphic studies along the Nicoya Peninsula (e.g., Hare and Gardner, 1985; Marshall and Anderson, 1995; Gardner et al., 2001; Marshall et al., 2012) have recognized two significant breaks in upper-plate topography and tectonic uplift that most likely relate to the subducting seafloor boundaries offshore. While the southern topographic break is coincident with the CNS-1 to CNS-2 transition, the northern geomorphic transition occurs some 30 km north of the mapped location of the offshore EPR/CNS-1 boundary. Interestingly, a sharp jump in the up-dip depth of subducting plate

seismicity (Newman et al., 2002) also occurs beneath the geomorphic break in surface deformation [Figure 6]. This project will attempt to further reconcile this discrepancy and locate more precisely the break in upper-plate deformation as shown by marine terraces.

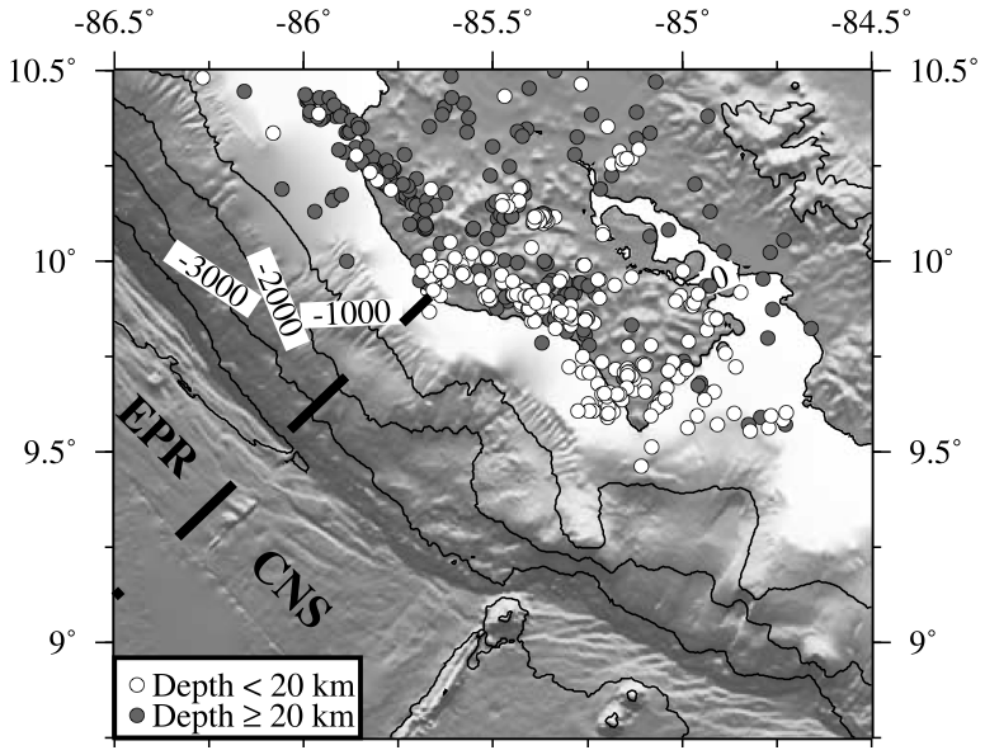

Figure 6: Distribution of subduction interface earthquakes along the Nicoya Peninsula (Newman et al., 2002). An abrupt shift in the depth of the updip limit of seismicity can be observed at a location approximately 30 km northwest of the mapped trace of the EPR-CNS boundary.

Geomorphic Surfaces

Ongoing tectonic uplift of the Nicoya Peninsula forearc has been documented through the study of uplifted marine and fluvial terraces (e.g., Hare and Gardner, 1985; Marshall and Anderson, 1995; Gardner et al., 2001; Marshall et al., 2012; Morrish, 2015). These terraces occur within a system of regional geomorphic surfaces mapped throughout the peninsula [Figure 7]. By constraining surface elevations and ages, prior workers have been able to determine rates of surface uplift and tilting along the Nicoya coastline.

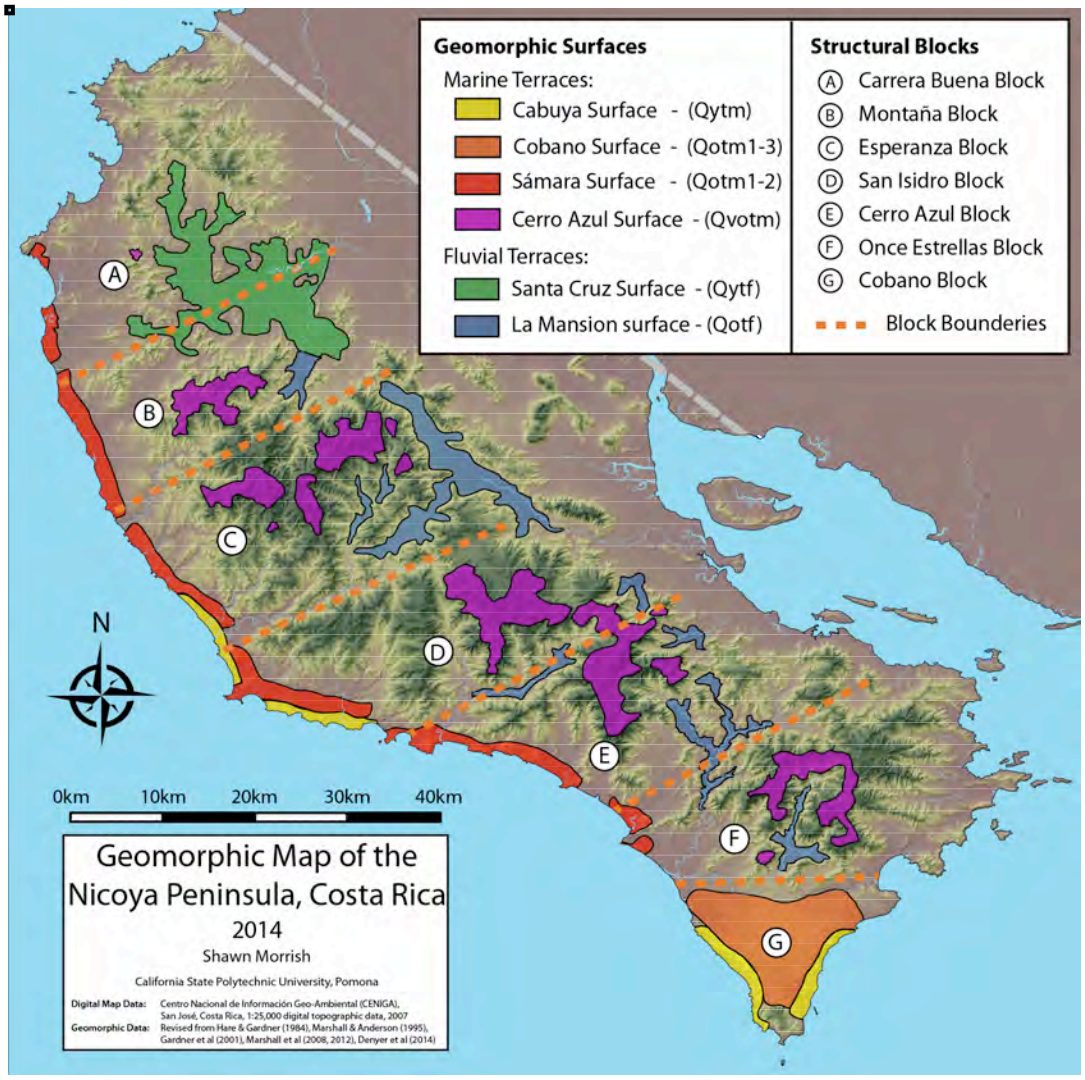

Figure 7: Geomorphic Map of the Nicoya Peninsula (Morrish, 2015).

Two major Quaternary geomorphic surfaces occur along the southeastern shoreline of the Nicoya Peninsula [Figure 7]. The upper surface, called the Cobano terrace (Hare and Gardner, 1985), is a deeply incised coastal terrace that averages 180 meters in elevation and is found overlying large abandoned sea cliffs. The Cobano surface was formed by uplift beginning in the middle Pleistocene that led to terrace erosion during the maximum late-Pleistocene eustatic sea level stand (stage 5e) at 125ka (Marshall et al., 2010). The Cobano surface is cut into the Montezuma Formation, a

Miocene to Pleistocene age marine sandstone that is indicative of a depositional environment that was becoming progressively shallower (Marshall & Anderson, 1995).

The lower surface that is visible along the southeastern shoreline of the Nicoya Peninsula [Figure 7] is called the Cabuya surface (Marshall and Anderson, 1995). The Cabuya surface is a low-lying Holocene wave-cut terrace that lies between the abandoned Cobano sea cliffs and the modern shoreline. Averaging less than 20 meters in elevation and less than 1 kilometer in width, the Cabuya surface is a relatively narrow surface that corresponds with a late Holocene age of <7ka. The Cabuya surface was cut into the basalts of the Nicoya Complex and overlying marine sedimentary rocks (Marshall & Anderson, 1995).

As one moves further northward up the western coastline of the Nicoya Peninsula, the Cobano surface drops in elevation to <50 meters and changes in name to the Sámara surface (Denyer et al., 2014). The Sámara surface has been referred to in previous literature as the Iguanazul, Carrillo, and Carrillo-Camaronal surfaces (Marshall et al., 2008, 2010, 2012). The Sámara surface is equivalent in age to the Cobano surface, but is found at much lower elevations, averaging 20-40 meters in elevation above modern sea level.

The Cerro Azul Surface is a high elevation (up to 900m) marine erosional surface (Hare and Gardner, 1985) that can be found capping the interior mountains that run the length of the Nicoya Peninsula. It is a deeply weathered surface, bounded by a prominent topographic scarp with up to 250-meters of relief. The scarp is continuous over many kilometers and causes consistent changes in streams and drainage basins across the

Peninsula. The surface is split into 6 major blocks that vary in elevation and reflect anticlinal structure of the peninsula (Hare & Gardner, 1985).

In addition to the Quaternary marine terraces, fluvial terraces can also be found along the length of the Nicoya Peninsula [Figure 7]. Two major fluvial surfaces have been identified (Hare and Gardner, 1985), the Pleistocene La Mansión surface within interior valleys, and the Holocene Santa Cruz surface on the northern interior plains.

While all of these terrace surfaces have been mapped in a regional sense, most elevation and age data are site specific, based on field surveying and isotopic dating. The goal of this research project is to apply ArcGIS methodology to develop Digital Terrain Models and continuous terrace surface maps to extract elevation data from areas that have not been studied in detail in the field. It is important to keep in mind that other geomorphic features, with morphologic characteristics similar to marine terraces, can also be found on the Nicoya Peninsula. While a surface may be identified in this project as a potential marine terrace, further field verification may be necessary on a case-by-case basis.

.

METHODS

The procedure that follows used ESRI ArcMap software to map the different levels of uplifting marine terraces along the western coast of the Nicoya Peninsula and used the resultant map to estimate the inner-edge elevations of these terraces. The GIS procedure developed in this paper is derived from a similar procedure developed for marine terraces on Santa Cruz Island, California by Scott and Pinter (2003).

Marine terraces are relatively flat surfaces that encompass an area containing similar values of elevation. Thus the procedure used here queries both slope and relief DTMs for cell values that may indicate a flat, continuous surface. Each query produces a map of cells that might correspond to areas containing marine terraces. These maps are referred to in this study as "extract maps." The extract maps produced by each query were compared to prior terrace maps (Marshall et al., 2008, 2010, 2012) created from both field data and aerial photos, to determine which query was the most successful. Ultimately, the most successful query will be used to estimate terrace inner-edge elevations (i.e. paleo-shorelines at late Quaternary sea level maxima).

DATA SOURCES

Digital Topographic Data

The digital source datasets used to create the DEMs and DTMs in this project were generated by the Costa Rican National Center for Geo-Environmental Information (CENIGA). CENIGA is a research center created in 2001 through a partnership between the Costa Rican Ministry of Environment and Energy (MINAE) and the government owned Petroleum Refinery (RECOPE) with the purpose of acquiring, managing, and disseminating environmental data and information. To achieve this goal, CENIGA is

developing an integrated GIS-based National Environmental Information System (SINIA). One of the products that CENIGA has worked to generate is a new, high-resolution, digital topographic database for Costa Rica. This database is derived from new aerial photographs (1:40,000 scale) that were ortho-rectified using the national topographic database (Instituto Geografico Nacional - IGN). Digital elevation datasets were then extracted through stereo-photogrammetric analysis and were then used to generate a new, country-wide set of digital 1:25,000 scale topographic maps (with 10 meter contour interval) that replaced the previous IGN 1:50,000 scale quadrangles (20 meter contour interval).

Initial Field Data

The abrupt tectonic segmentation of the subducting Cocos plate has made the Nicoya Peninsula the target of a series of geomorphic studies over the past few decades, several of which provided the raw field data used in this project (Marshall et al., 2008, 2010, 2012). The earliest studies characterized the regional geomorphic surfaces and overall deformational structure of the peninsula (e.g., Hare and Gardner, 1985). Later studies focused on the rapid coastal uplift and tilting at the peninsula's southern tip (e.g., Marshall and Anderson, 1995; Fisher et al., 1998; Gardner et al., 2001). Further research extended the marine terrace uplift record along the entire western coast of the Nicoya Peninsula (e.g., Marshall et al., 2008, 2010, 2012; Sak et al, 2009; LaFromboise, 2012). Some of these studies also correlated uplifted marine terraces at the coast with fluvial terraces within inland valleys (e.g., Hare and Gardner, 1985; Marshall et al., 2010; Morrish, 2015).

Detailed site-specific data was collected on uplifted Nicoya Peninsula marine and fluvial terraces at seven coastal study sites [Figure 8] as part of a 2010-2012 NSF MARGINS research project (Marshall et al., 2010, 2012). The seven coastal field sites were selected to correspond with the seven structural blocks identified in earlier studies by Hare and Gardner (1985).

Terrace surfaces at each site were mapped in the field on 1:25,000 scale topographic maps. Topographic profiles were surveyed across terraces using eye-level and stadia rod for short transects, and differential barometric altimetry for long transects. Handheld GPS units were used to determine survey locations and distances. Samples were collected from terrace deposits and terrace tread surfaces for age dating using cosmogenic radionuclides (CRN), optically stimulated luminescence (OSL), and radiocarbon (^{14}C). Additional age determinations were made by correlating terrace inner edge elevations with paleo-sea level curves (LaJoie, 1986). The resulting terrace data from five of the coastal study sites (Sites 2, 3, 5, 6, & 7) was used in this project to calibrate the DTM analyses [Figure 8, Appendix B].

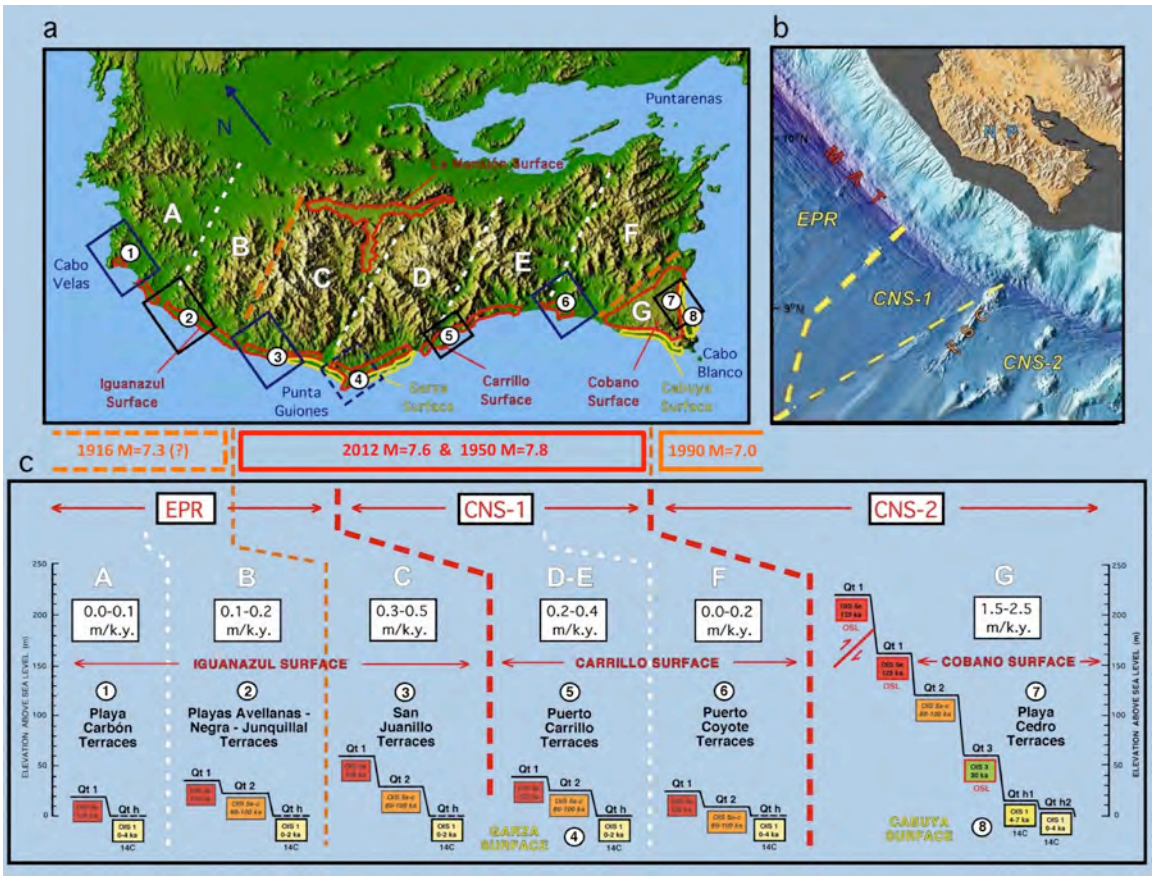

Figure 8**:** a) Digital elevation model of the Nicoya Peninsula (NASA-SRTM) showing areas of uplifted marine and fluvial terraces within the late Pleistocene Iguanazul, Carrillo, Cobano, and La Mansion geomorphic surfaces (red outlines); and the Holocene Garza and Cabuya surfaces (yellow outlines). Rectangles outline the coastal study areas. Dashed white lines mark prominent structural lineaments that form the boundaries of 7 interior mountain blocks (A-G) with varying topographic relief. b): DEM of Nicoya convergent margin showing location of Middle America Trench (MAT) and three distinct domains of subducting Cocos Plate seafloor: EPR, CNS-1, CNS-2. c): Summary diagram showing uplifted coastal terrace elevations, age data, and uplift rates within each study area. Numbers in circles indicate specific study sites for Pleistocene and Holocene terraces. Terrace ages are based on sea level curve correlations and isotopic dates (OSL, TCN, and 14C, as indicated). The highest uplift rates occur within block G directly inboard of subducting CNS-2 seamounts. Outside of this area, the most rapid uplift occurs in blocks C-E inboard of CNS-2 and EPR crust and above the 2012 M7.6 and 1950 M7.8 earthquake rupture zones (indicated by box at top). An abrupt decrease in uplift rate occurs northwest of these earthquake rupture zones across the lineament separating blocks B and C. This suggests that the northwestern end of the peninsula may lie within a distinct seismogenic zone segment of the plate margin (Figure after Marshall, 2012).

DATA PROCESSING

Initial GIS Datasets

The initial assessment of the topographic data showed ten errors that needed to be resolved before any further processing could occur. These ten errors consisted of six files that had undefined coordinate reference frames and could not be properly supported by the software, and four files that were duplicates. The duplicated files were deleted, after a check to ensure that the files were in fact duplicates of existing files. A less common error would have been unique files that were displaced to overlap with preexisting files, rather than identical information duplicates. The files with undefined coordinate frames were a quick fix that just needed to be defined, after checking that their current locations were indeed correct. A total of 99 separate topographic quadrangles were used to create the overall shape of the Nicoya Peninsula in this project.

TIN Versus DEM Processing

The initial topographic data were contour datasets that display elevation data as vector map files, but are not capable of further manipulation. To manipulate elevation data to determine other values, like slope and relief, the initial contour data had to first be converted into a continuous surface, so the breaks in the contour lines between each map quadrangle wouldn't skew the creation of surfaces. There are two main continuous surface types that can be created are called Triangular Irregular Networks (TINs) or Digital Terrain Models (DTMs). TINs are better at shape identification, because of the irregularly sized triangular cells, but can cause artificial terraces to form. DTMs do not create as precise of shape forms, because of the identically sized square cells used for processing, but does not cause artificial terraces to form and therefore has much better

slope processing potential. Since this project is looking at identifying and classifying terraces, Digital Terrain Models were created from the initial contour data.

Digital Terrain Models

Elevation and other topographic variables, such as slope and aspect, can be displayed in digital maps called Digital Terrain Models, or DTMs (Florinsky, 1998). Most often, DTMs are created in a raster (random regular grid) format, which means that the topographic variable is displayed in a grid of regularly spaced samples, or cells, with the same distance of separation in both the x and y direction (Guth, 1995). The nature of a raster grid allows for calculations to be applied easily to DEMs, converting elevation data into a number of other values (e.g. slope), thus creating new DTMs (Florinsky, 1998). While the even grid spacing allows for quick and useful data manipulation, it does not allow for variability of sampling, or cell size, across complicated terrain. This leads to either oversampling of values across consistent terrain or under-sampling of values across complicated terrain (Bolstad, 2007), a choice that can greatly affect processing time of data collected.

DTMs are a commonly used data source in many studies. Elevation data and the derived surfaces are used in many fields of study, including hydrology, geology, public transportation, ecology, and urban planning. These fields and many others use a variety of tools called geographic information systems (GIS) where digital terrain models can be viewed and processed. DTMs have been used to identify and characterize streams (Ijjasz-Vasquez and Bras, 1995), mountains (Guth, 1995), estimated erosion (Florinsky, 1998), marine terraces (Scott and Pinter, 2003), and fluvial terraces (Morrish, 2015), amongst other studies.

Creation of DEMs

Digital Elevation Models (DEMs) are a specific type of DTM that contains elevation data (Florinsky, 1998). For large sets of data, separate DEMs can be created for each initial file, or one large DEM can be created for the entire dataset. Separate DEMs have smaller file sizes and take much less time and much less computer memory when processing. One large DEM can take lot more processing time, but helps smooth over errors that could occur at the boundaries between files.

Initially, one large DEM of the Nicoya Peninsula was created, however, a processing error was encountered. The conversion from vector contour data to raster DEM extrapolated outwards from the initial peninsula shape, to a rectangle that encompassed the peninsula. To rectify this problem, a generic outline of the peninsula was created, which was used to define the total extent of the area that should be processed in the formation of the DEM. This boundary stopped the extrapolation of elevation values outside of the peninsula.

Determining the appropriate cell size to use is a very important step that affects both the resulting map and the processing time for the rest of the project. Too few cells, and the resulting DEM will smooth over details present in the original data. Too many cells and you risk artificially creating features that are not present in the original data. By determining the number of cells created, cell size also directly affects the processing time; cutting the cell size by one-half forms four times as many cells and leads to four times the processing time. All cartographers agree that cell size is extremely important, but they disagree on resolution.

The initial contour datasets come from a 1:25,000 scale topographic map, which limits the resolution of individual cells. According to Tobler (1988), map scales should be converted from map scale to cell size using the following equation:

$$Cell\ Size = \frac{Map\ Scale}{1000 \times 2}$$

For the 1:25,000 scale Costa Rica datasets, this allows for a minimum cell size of 12.5-meters. In contrast, the Peuker criterion states that a DEM grid size should be 4.3 times larger than the contour interval (Florinsky, 1998), which would necessitate a cell size of 43 meters. Other cartographers believe that features as small as 3-5 meters across can be identified on a 1:25000 scale map, and a smaller cell size should be used (Frye, 2007). All scientists agree that it is important that the DEM resolution is not higher than the resolution of the source materials (Florinsky, 1998), in this case a 1:25000 scale map. For the purposes of this project, a 12.5 meter cell size was used according to Tobler (1988).

Slope & Relief DTMs

The Nicoya Peninsula DEMs [e.g. Figure 9] were converted into both slope and relief DTMs for the terrace extraction procedure. Slope DTMs [Figure 10] were created using the Slope GIS function in ESRI ArcMap's Spatial Analyst toolbar. The slope function calculates the maximum rate of change from a cell to each of its neighboring cells. Slope values are given in degrees. The slope maps by themselves are not enough to determine the locations of terraces. Other areas of low slope (e.g. canyon floors, ridge tops, etcetera) will create a false positive response and need to be removed. Such false positive cells were removed by creating maps that denote the relief in an area, or the change in elevation. Relief DTMs [Figure 11] were created for the procedure by

calculating the maximum change in elevation at each cell, by comparing each cell to cells around it within a certain radius. This operation used the Focal Statistics tool in ArcMap's Spatial Analyst Toolbar. The circular windows queried had radii that were multiples of cell size. Radii ranged from 2-12 cells in size, or 25-150m.

Figure 9: Elevation DTM at Carrillo (Study Site 5, Figure 8). Cell Size, 12.5m. Elevation ranges from low (dark green; -90 meters) to high (purple; 773 meters).

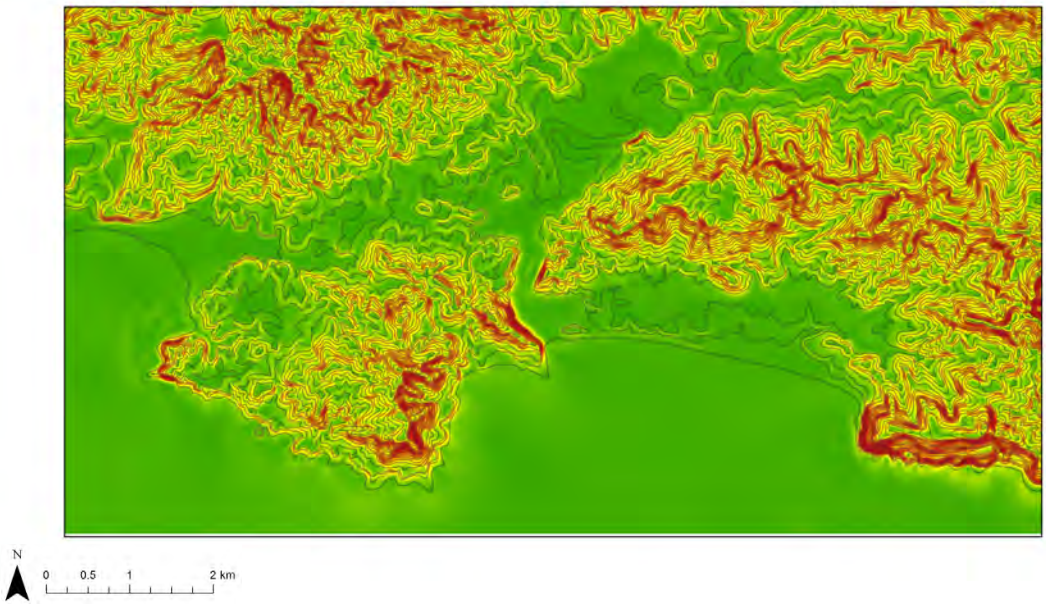

Figure 10: Slope DTM at Carrillo. (Study Site 5, Figure 8). Cell size, 12.5m. Slope values range from low (green; 0º slope) to high (red; 58.4º slope).

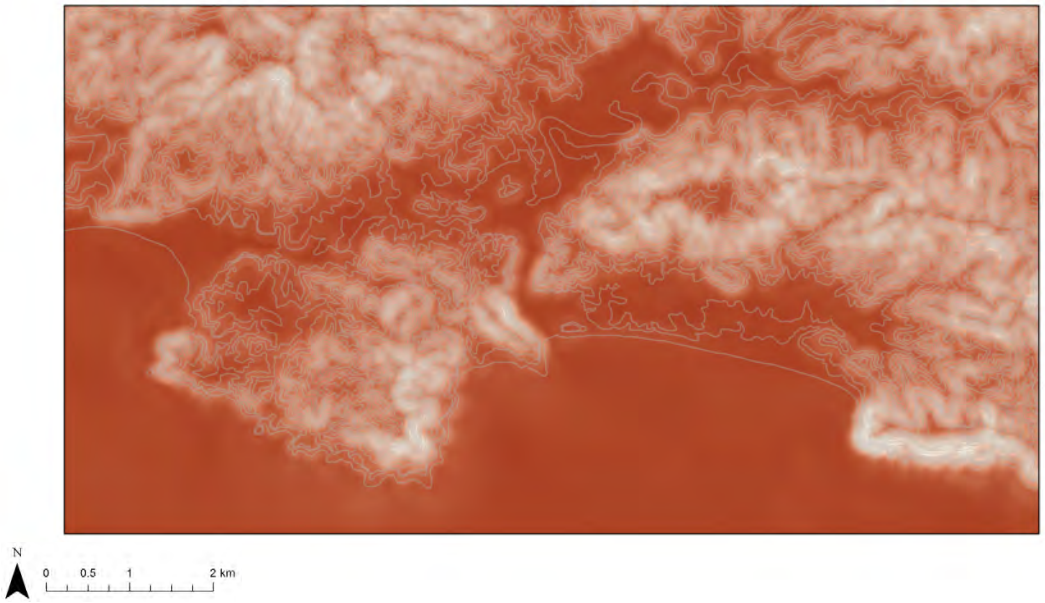

Figure 11: Relief DTM at Carrillo. (Study Site 5, Figure 8). Cell size, 12.5 m. Releif values range from low (dark red; 0 meters relief) to high (white; 250 meters relief) over a selected radius.

Creation of Rasterized Terrace Maps

Field –based terrace maps from five distinct locations along the Nicoya Peninsula (Marshall et al., 2008, 2010, 2012) were used to check the success of the terrace extraction procedure. The field datasets were first digitized using ArcMap, and then aerial photos were used to add in the inferred locations of modern beaches. At two of the five locations, a large river reached the coast and the river mouths were also digitized. The procedure adapted from Scott and Pinter (2003) that was used to extract potential terrace locations is designed to exclude other relatively level landscape features, such as small streambeds, canyon bottoms, ridge tops etcetera, but the effect of larger riverbeds on the procedure was unknown, so large river mouths present at field locations were also digitized using ArcMap. Once all these features were digitized, the terrace maps were converted into raster format. Each raster cell was assigned a numerical value, rather than a text value, to allow for easier manipulation of the raster datasets. Mapped terraces given a value of two, inferred beaches given a value of four, large rivers given a value of six, and all other cells given a value of zero.

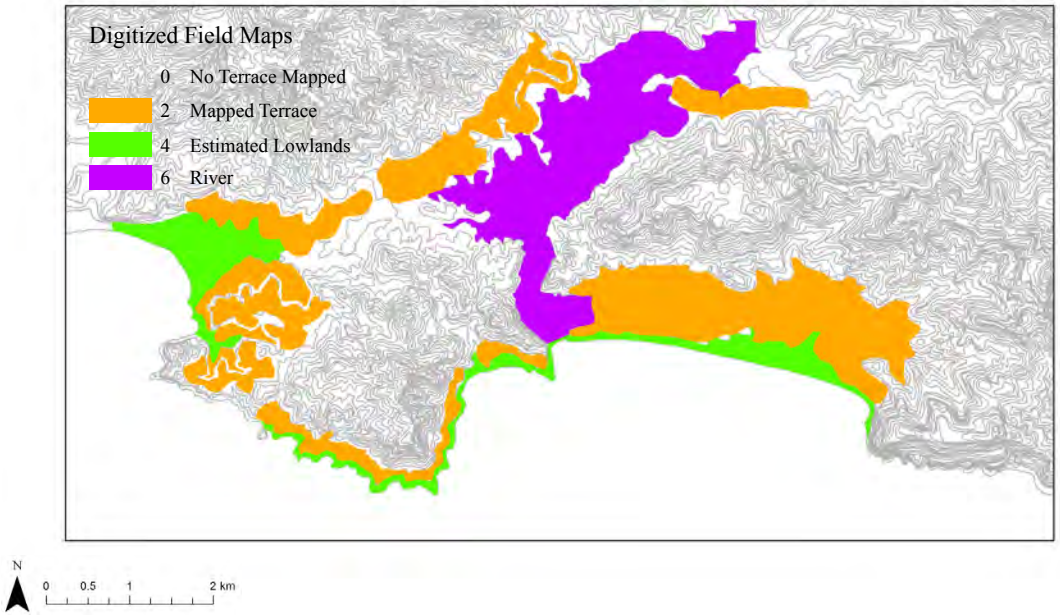

Figure 12: Rasterized Field Map at Carrillo (Study Site 5, Figure 8).

Terrace Extraction Procedure

Slope and relief DTMs were both queried simultaneously in order to find the combination of input parameters that was the most successful at extracting marine terraces. Relatively gently sloping areas of land are indicative of marine terraces, so slope DTMs were queried for cell values ≤ 5º, 10º, and 15º. Similarly, marine terraces are fairly continuous and needed to be distinguished from other flat areas, like stream beds and ridge tops, so areas of low relief, or little elevation change, were targeted using relief DTMs. Relief DTMs were queried for values of ≤ 5, 10, 15, 20, and 25 meters of elevation change across DTMs calculated over circular windows with radii of 25, 37.5, 50, 62.5, 75, 87.5, 100, 112.5, 125, 137.5, and 150 meters. The original DEMs were also queried to ignore any coastal elevation less than zero. The initial search algorithm was as follows:

[DEM ≥ 0m and slope ≤ 5º and relief (25m-radius) ≤ 5m]

Each iteration yielded an extract map [Figure 13] where a value of zero indicates no terrace found at that cell and a value of one indicates a potential terrace location.

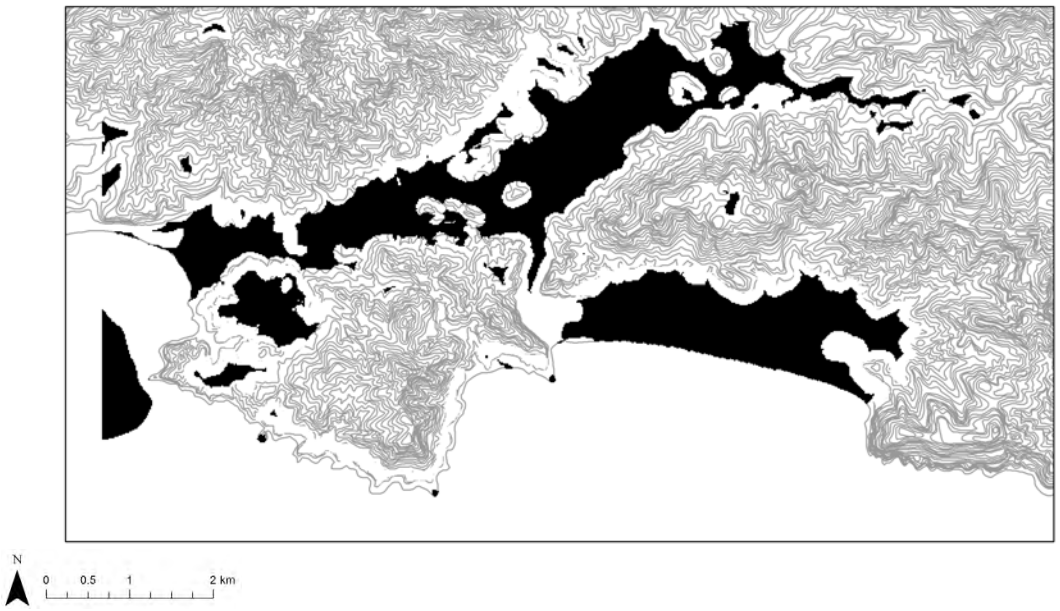

Figure 13: Extract Map at the Carrillo location (Study Site 5, Figure 8). Created using the Raster Calculator in ArcGIS. Values of 1 (shown in black) indicate the location of a potential terrace. Values of 0 (no color) indicate that no terrace was found at that point.

Error Maps

Based on the methods of Scott and Pinter (2003), each of the iterations needed to be processed further to determine a numerical representation of success. The calculation for success compares the potential terrace locations yielded by the extract maps (value of 1 for potential terrace; value of 0 for no terrace found; Figure 13) to the field-mapped terrace data (values of 2, 4, and 6; Figure 12) at each raster cell. When these two maps were added together using the Raster Algebra tool in ArcGIS, an error map [Figure 14] was created with values from 0-7 populating each cell.

A value of 0 indicated that there was no terrace found in the extract map and no surface mapped on the field map. A value of 1 indicated that a potential terrace was found on the extract map, but it matched no surface on the field map. A value of 2 indicated that a terrace was mapped on the field map, but no matching potential terrace was found on the extract map. A value of 3 indicated that a potential terrace surface was found in the extract map and it matched a mapped terrace in the field map. A value of 4 indicated that a beach or coastal lowland surface was mapped on the field map, but no matching potential surface was extracted. A value of 5 indicated that a potential terrace surface was found on the extract map that corresponds to a mapped beach surface on the field map. A value of 6 indicated that no potential terrace surface was found in a location with a mapped riverbed. A value of 7 indicated that a potential terrace surface was found in a location matching a mapped riverbed. Attribute tables [Figure 15] within ArcGIS provided counts of the number of cells corresponding with each value. These cell counts were used to calculate values that would determine the success of each set of initial parameters.

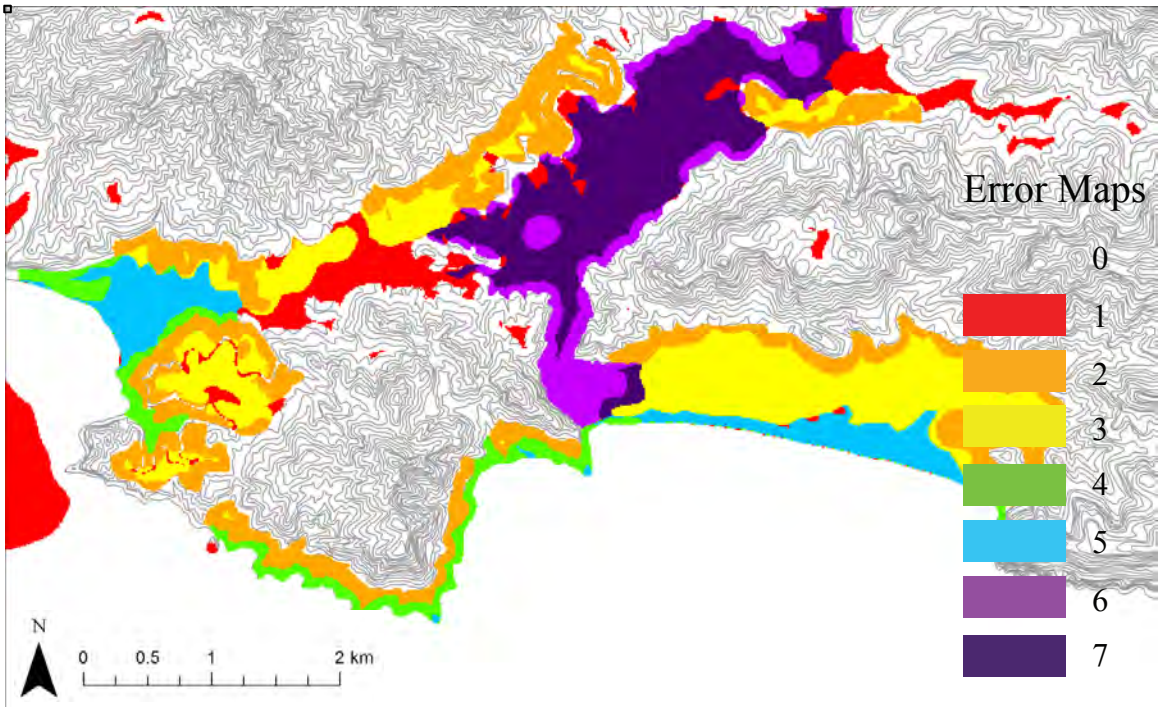

Figure 14: Error Map at Carrillo (Study Site 5, Figure 8).

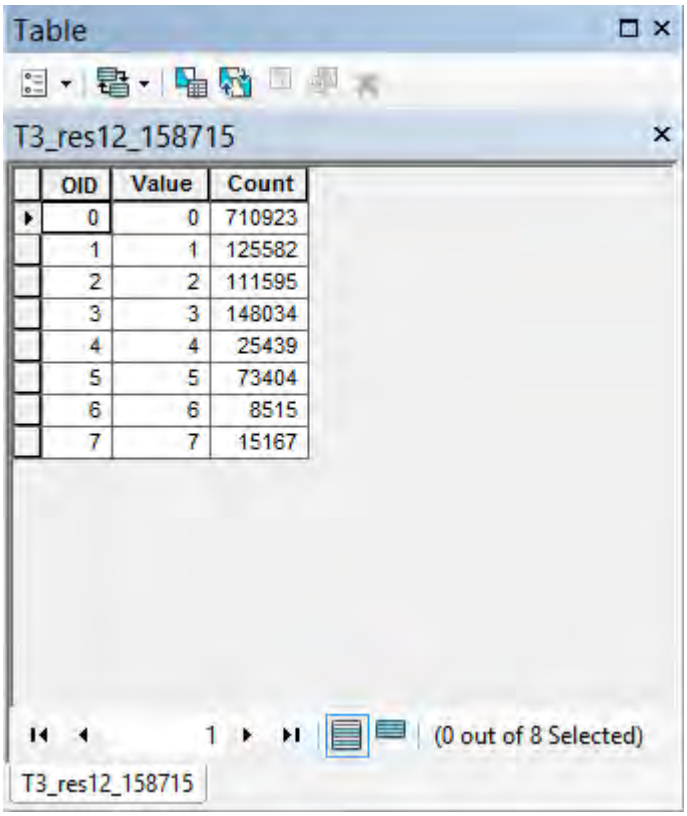

Figure 15: Example of the Attribute Table within ArcGIS. These cell counts were used to calculate success values at each set of input parameters.

Match, Oversample, and Undersample

When comparing a specific raster cell within the extract maps to the same raster cell within the corrected field maps, there are three possibilities that can occur.

1) The two cells can match one another, if both maps indicate that there is a terrace within that cell. Scott and Pinter (2003) refer to these cells as coincident cells.
2) The two cells do not match: the extract map found a terrace at that cell, but there was not one a terrace indicated in that cell on the corrected field map. Scott and Pinter (2003) refer to this as an error of commission, or oversample.
3) The two cells do not match: the extract map did not find a terrace at that cell, but there was a terrace indicated in that cell on the corrected field map. Scott and Pinter (2003) refer to this as an error of omission, or undersample.

Values of Success

Once the extract maps had been created for each combination of input values, and each cell had been classified as match, oversample, or undersample, the value of success for each location needed to be calculated according to the following equation by Scott and Pinter (2003):

$$\frac{M - O}{M + U}$$

Where extract map cells are sorted into three categories: match (M), oversample (O), and undersample (U). This equation automatically takes into account the total amount of cells mapped on the corrected field maps, because the sum of the match cells (M) and the undersample cells (U) equals the number of field cells. Therefore this ratio of match over field cells automatically is determined relative to the amount of

undersample cells. The equation also corrects for oversample cells, which means that large negative values of success are possible when running initial values that create large regions of oversample cells.

Four Trials for Terrace Extraction

Once success was calculated at the test sites, the final choice was to accept the results, or adjust the procedure prior to moving on to the calculation of a correction factor. This choice led to a series of three trials to determine how to best extract terraces using the mapped data.

Trial 1: This trial focused on using the marine terrace data exactly as mapped, without considering other large gently sloping surfaces like unmapped modern beaches and large rivers within the field area. The unmapped beaches and river terraces skewed the results of the experiment because the better fitting iterations led to too many oversampled cells within the mapping area, by picking up the presence of those unmapped features. Therefore the most successful iteration yielded was the one with the least amount of oversample, which in this case meant that the iteration picked very few surfaces as potential terrace locations.

Trial 2: This trial focused on adding unmapped beaches to the existing mapped data. Using aerial photographs and following contours, unmapped beaches were added to the field data. This trial allowed for higher success rates at the field sites, but also caused higher success values at the locations with the most modern beaches, because the iterations yielded a higher quantity of cells that matched the modern beaches than cells that that matched the mapped terraces.

Trial 3: This trial focused on adding both unmapped beaches and unmapped rivers to the existing mapped data. Using aerial photographs and following contours, unmapped beaches were added to the field data. Large rivers were also traced and added to the data as potential terrace locations. This trial allowed for much higher success rates at the field sites, but again skewed the results of the experiment. Success rates were skewed towards the iteration that best fit the river, as the feature of largest area, when in truth the river should not be an entire terrace, but a feature associated with terraces instead.

Trial 4: This trial focused on adding unmapped beaches to the existing mapping area, while removing large water features from the testing area entirely. The regions of the map associated with water were removed after Trial 2, so that the larger rivers and fluvial terraces associated would not affect the success values. This was done in the hope that whatever iteration was most successful might still pick up on river terraces, but without skewing the success rates through undersample (Trial 2) or oversample (Trial 1).

Trials 2, 3, and 4 [Figure 16] have visually similar results, but Trial 3 had the most success, with the initial parameters of slope $\leq 15^{\circ}$, and relief $\leq$ 15m across a radius of 87.5 meters (7 cells).

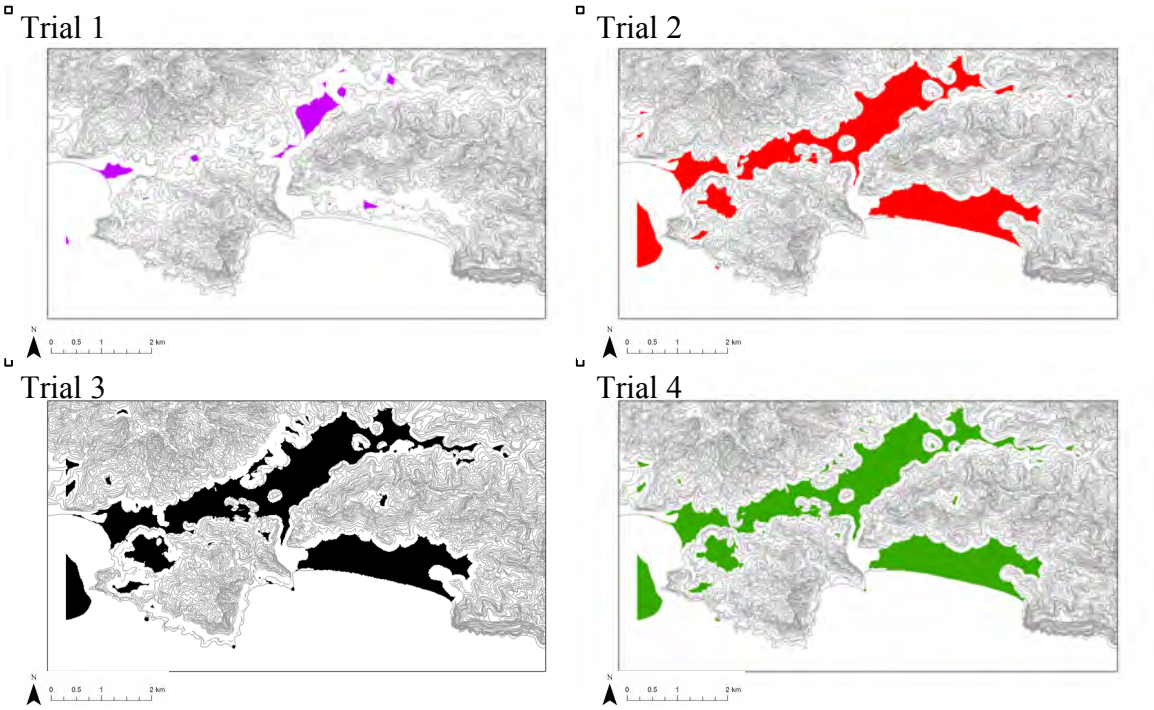

Figure 16: A sample set of results found when running all four trials at the Carrillo location (Study Site 5, Figure 8). Trials 2, 3, and 4 all had very visually similar terrace extract maps with the highest values of success. Trial 1, however, had so much potential for oversample that the result with the best success calculation tended to pick up very few surfaces.

DISCUSSION OF EXTRACT MAPS

The sections that follow summarize the results found at each field site (Figure 17; Sites 2, 3, 5, 6, 7) including a physical and geographic description of each site, the success values at each site, and a comparison of field mapped terrace transects versus the digitally extracted terrace transects.

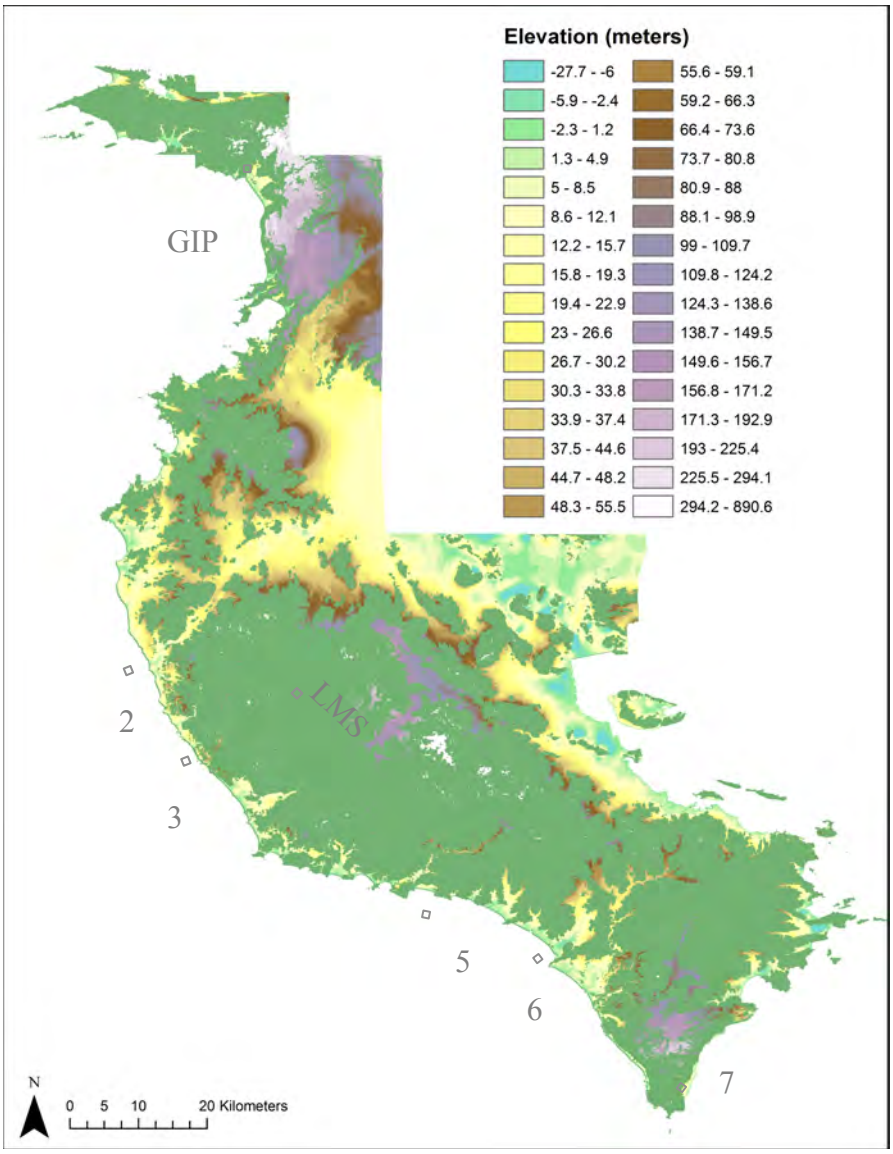

Figure 17: The extract map above shows the extracted terrace map across the entire peninsula. Grey boxes show sites of interest: Field Sites 2, 3, 5, 6, and 7; the La Mansion Surface (LMS); a Guanacaste ignimbrite plateau (GIP).

SITE #2: Villareal

Site 2 is the northernmost field site [Figure 17] along the Nicoya Peninsula used to test and calibrate the marine terrace extraction procedure. Several beaches can be found at Site 2, including Playa Avellanas, Playa Negra, and Playa Pochotes. Two tiers of marine terraces, Qt1 and Qt2, are well expressed at Site 2. These two tiers make up the Pleistocene Sámara surface. While some stretches of modern coastline were estimated at this location between the lower terrace (Qt2) and the ocean, little alteration to the original field map was necessary at Site 2. The terrace extraction procedure at Site 2 extended the upper Sámara terrace (Qt1) to a higher elevation [Figure 18] than that of the original field map, but otherwise was highly successful.

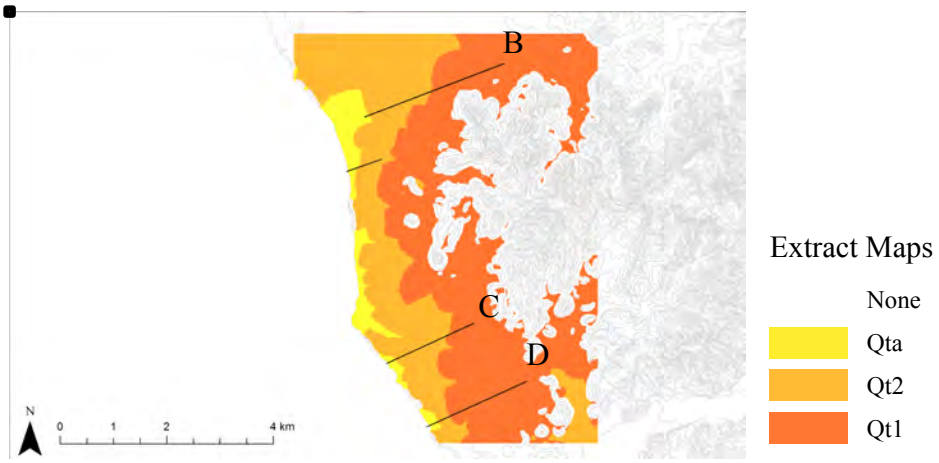

Figure 18: Extract Map at Villareal, showing different terrace surfaces Qta, Qt2, and Qt1 as estimated based on elevation and extracted Transects B-D (Study Site 2, Figure 17).

SITE #3: Cerro Brujo

Site 3 lies just to the north of the EPR/CNS-1 boundary [Figure 17] near San Juanillo. Three smaller rivers reach the Pacific Ocean along this stretch of coastline and both terraces found within the Sámara surface (Qt1 and Qt2) are preserved at Site 3. Small portions of coastal lowlands (e.g. beach, wetland, floodplain) and river mouths were estimated at Site 3, but the rivers at this location had relatively small (>1km) floodplains that did not skew the success calculations greatly at this location. Of the three rivers, only fluvial terraces associated with Río San Juanillo were extracted, while the marine terraces themselves were well modeled [Figure 19].

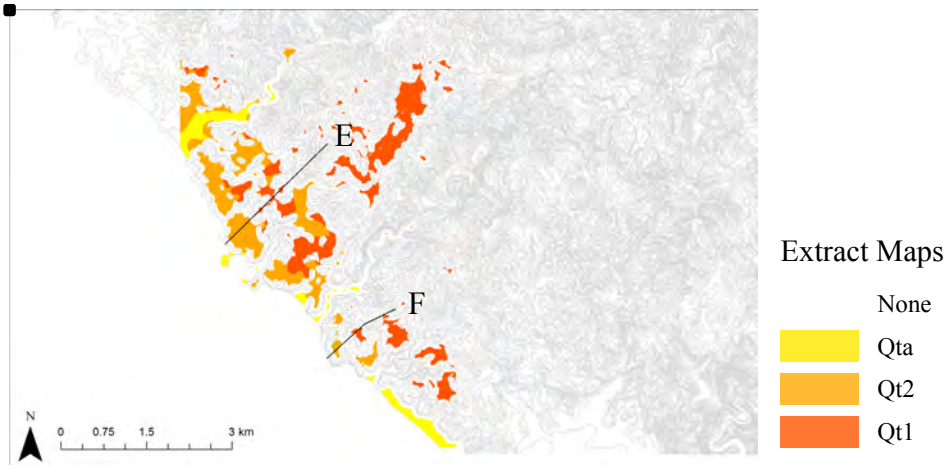

Figure 19: Extract Map at San Juanillo, showing different terrace surfaces Qta, Qt2, and Qt1 as estimated based on elevation and extracted Transects E-F (Study Site 3, Figure 17).

SITE #5: Cerro Azul

The two marine terraces (Qt1 and Qt2) within the Sámara surface are also preserved at Site 5, near the middle of the Nicoya Peninsula's coast [Figure 17] along Playa Carillo and Playa Camaronal. Site 5 is marked by unique topography associated with Río Ora, a large river that used to reach the Pacific Ocean at Playa Carrillo, but has been cut off and now exits at Playa Camaronal (Morrish, 2015). The Río Ora is bounded by a large floodplain (around 1 km across) that was estimated as an initial parameter to reduce the amount of oversample found at this location (Appendix A). The extraction procedure was successful in picking up many surfaces [Figure 20] near Site 5, including the two marine terraces surfaces of interest as well as the modern beach and fluvial terraces corresponding to the Río Ora floodplain.

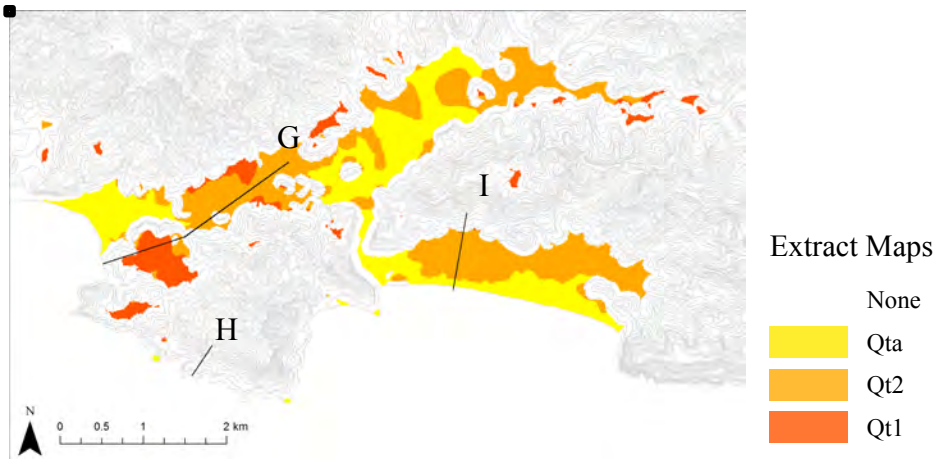

Figure 20: Extract Map at Carrillo, showing different terrace surfaces Qta, Qt2, and Qt1 as estimated based on elevation and extracted Transects G-I (Study Site 5, Figure 17).

SITE #6: Puerto Coyote

Only one Sámara terrace (Qt1) can be seen at Site 6 [Figure 17] towards the south of the Nicoya Peninsula along Playa Coyote. Site 6 is dominated by a large floodplain associated with Río Jabillo bounded on each side by the Sámara marine terrace. The modern beach and river mouth were estimated as initial parameters for the extraction procedure at this location, because initial trials ended with negative values of success due to a large amount of oversample attributed to the river mouth [Appendix A]. The extraction procedure was successful in picking up many surfaces [Figure 21] near Playa Coyote, including several river terraces as one moves further inland up Río Jabillo.

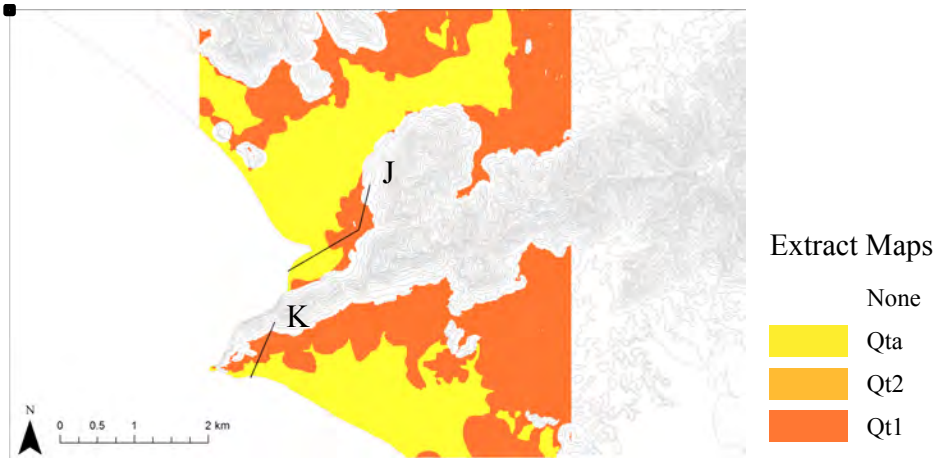

Figure 21: Extract Map at Puerto Coyote, showing different terrace surfaces Qta, Qt2, and Qt1 as estimated based on elevation and extracted Transects J-K (Study Site 6, Figure 17).

SITE #7: Cabuya

The Cobano terrace sequence (Qt1, Qt2, and Qt3) can be seen at Site 7 [Figure 17] at the southernmost tip of the Nicoya Peninsula, as well as the Cabuya surface (Qth). Site 7 consists of Playa Cabuya, Playa Cedro, and Playa Montezuma, where the four distinct terrace tiers have been mapped (Marshall et al., 2012). The subducting seamount chain associated with the CNS-2 crust causes rapid uplift at Site 7, allowing for high cliffs and deeply incised streams. The deep incision associated with the streams at Site 7 did not allow the terrace surfaces to be well described by the extraction procedure. The Cabuya surface, a low lying Holocene surface adjacent to the modern beach, was well defined by the extraction procedure. The uppermost terrace (Qt1) of the Cobano surface was also well defined, but the middle terrace levels (Qt2 and Qt3) were only sporadically extracted due to smaller surface area and deep incision [Figure 22].

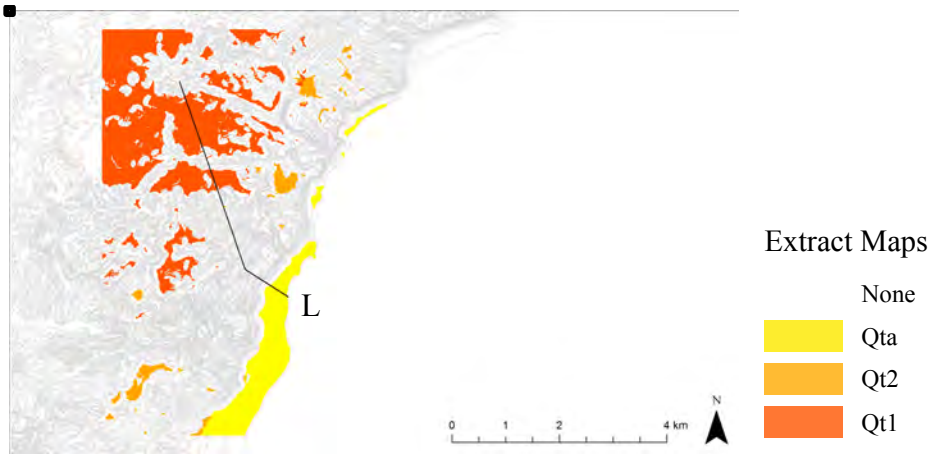

Figure 22: Extract Map at Cobano, showing different terrace surfaces Qta, Qt2, and Qt1 as estimated based on elevation and extracted Transects E-F (Study Site 7, Figure 17).

La Mansion Surface

The La Mansion surface is a fluvial terrace surface that forms a distinct T-shape [Figure 7]. The La Mansion surface is largely composed of stratified fluvial sands and gravels, whose clasts are derived from the Nicoya Complex (Hare and Gardner, 1985). This surface is a depositional terrace that creates large flat valley floors as a nearly continuous surface found 4-10 meters above stream level (Hare and Gardner, 1985). As a large, continuous, gently sloping surface, the La Mansion surface [Figure 23] was well depicted using the same extraction parameters used to model the marine terraces along the Pacific coast of the peninsula.

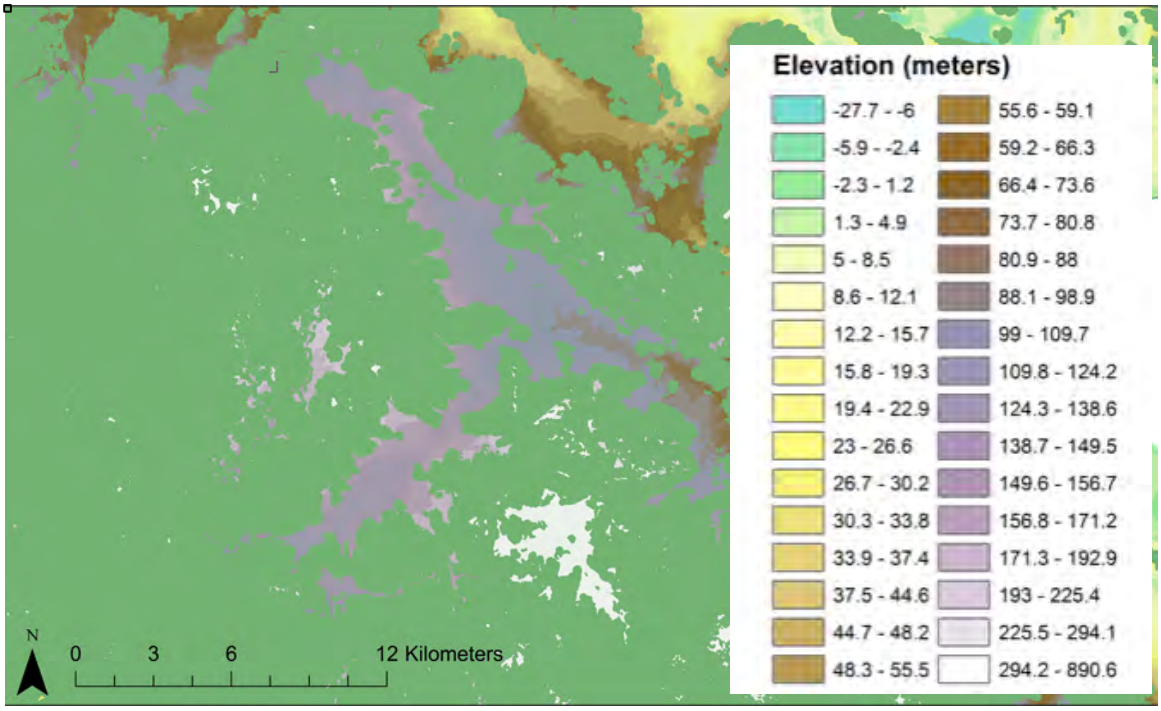

Figure 23: Extract map showing the La Mansion surface, a fluvial terrace that forms a distinct t-shape due to the surrounding topography.

Ignimbrite Deposit

At the northernmost extent of the project area, above the Nicoya Peninsula, a large surface was identified on the extract map that corresponds to a broad silicic ignimbrite plateau (2000 km^2), which can be traced inland to two remnant calderas within the Guanacaste Cordillera (Marshall, 2007). The plateau is a higher elevation surface than the target marine terraces, ending with a 100-meter high escarpment (Marshall, 2007) near the coastline. The Guanacaste ignimbrite flow forms a gently undulating plain (Marshall, 2007) that fits the parameters of the extraction procedure very well and allowed the flow to be picked up [Figure 24] while searching for marine terraces.

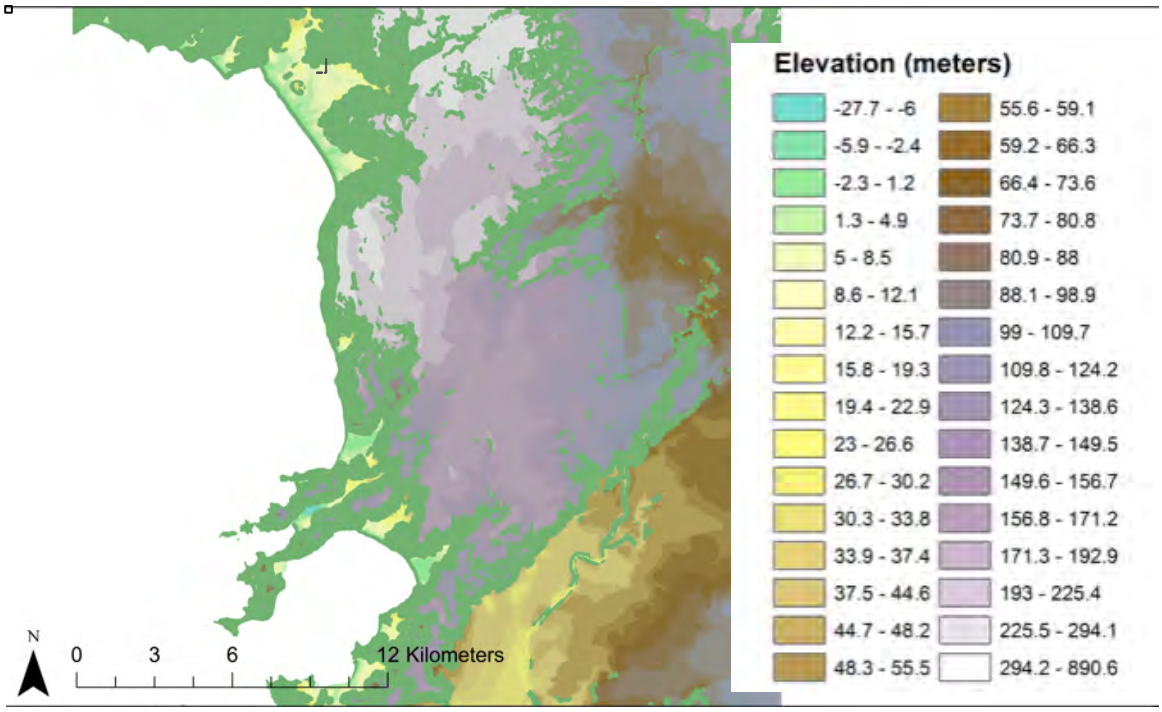

Figure 24: Extract map displaying a large ignimbrite flow to the north of the Nicoya Peninsula.

UPLIFT ACROSS THE NICOYA PENINSULA

CALCULATING MARINE TERRACE UPLIFT RATES

Coastal uplift rates can be determined using the modern inner edge elevation (Z) and the age (A) of uplifted marine terraces (Lajoie, 1986). This calculation requires knowing the elevation of the paleo-sea level high stand (z_{st}) during which the terrace formed as determined from the paleo-sea level curves (e.g. Imbrie et al., 1984; Rabineau et al., 2006). The uplift rate (R) is calculated using the following equation:

$$R = \frac{Z - z_{st}}{A}$$

EXTRACTION OF INNER EDGE ELEVATIONS

Before using DEM extracted inner edge elevations to calculate uplift rates, it is important to correct these values based on field measurements of actual terrace elevations. This approach uses an equation from Scott & Pinter (2003), where the field measured inner-edge elevations (Z_m) were compared with the mean DEM extracted inner-edge elevation (Z_e) and the standard deviation (S_e) at each field location, using the following equation:

$$Z_m = Z_e + cS_e$$

where you solve for the value of the coefficient c.

$$c = \frac{Z_m - Z_e}{S_e}$$

(Note that c can have a negative value if $Z_m < Z_e$)

The calculated values for coefficient c are listed in Table 1. The average correction value was 0.1860 (unitless). The average correction value for just the Qt1 terrace surface was -0.0213 (unitless). Considering the variance in the standard deviation

(S_e) at the different locations, the DEM extracted inner-edge elevations at any given Qt1 terrace location are on average somewhere between 0.8-0.28 meters higher than their field mapped counterparts, when the correction values are entered back into the equation above. This correction value is well within expected values, as an error of 2 meters or less is expected with a DEM created from a map with a contour interval of 10 meters (Florinsky, 1998).

Table 1: Elevation Correction Values

Site 2: Villareal					
	Terrace	Zm	Ze	Se	c
Transect B	Qt1	36.6	37.63	8.30	-0.1241
Transect C	Qt1	30	37.63	8.30	-0.9193
Transect D	Qt1	30	37.63	8.30	-0.9193

Site 3: Cerro Brujo					
	Terrace	Zm	Ze	Se	c
Transect E	Qt1	60	45.57	13.30	1.0850
Transect F	Qt1	60	45.57	13.30	1.0850

Site 5: Cerro Azul					
	Terrace	Zm	Ze	Se	c
Transect G	Qt1	30.9	31.22	10.73	-0.029822926
Transect G	Qt1	31.6	31.22	10.73	0.035414725
Transect I	Qt2	26.8	17.46	3.18	2.937106918

Site 6: Puerto Coyote					
	Terrace	Zm	Ze	Se	c
Transect J	Qt1	26.1	26.04	9.84	0.006097561
Transect K	Qt1	22	26.04	9.84	-0.410569106

Site 7: Cobano					
	Terrace	Zm	Ze	Se	c
Transect L	Qth	14.3	24.94	4.13	-2.576271186
Transect L	Qt3	61.3	55.77	9.32	0.593347639
Transect L	Qt2	143.8	133.59	6.17	1.654781199

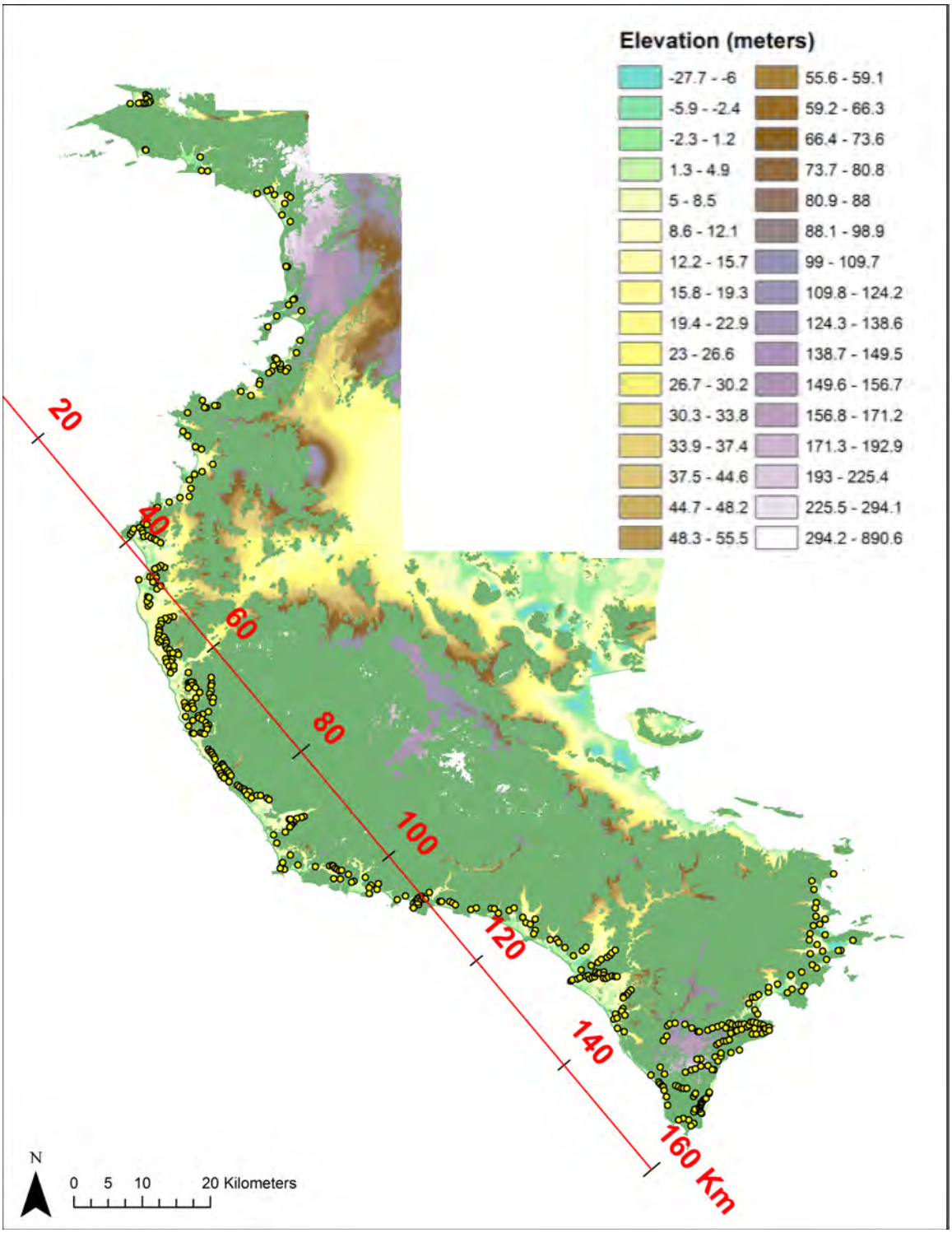

Figure 25: Yellow circles indicate sites where DEM extracted inner edge elevations were determined. Red line shows 130º trend line used to plot elevation values [Figure 28; Figure 29].

UPLIFT RATES ALONG THE NICOYA PENINSULA COASTLINE

The elevations of both erosional and aggradational geomorphic surfaces have long been used as a way to characterize tectonic uplift along the length of the Nicoya Peninsula (e.g. Hare and Gardner, 1985; Marshall and Anderson, 1995; Fisher et al., 1998; Gardner et al., 2001; Marshall et al., 2008, 2010, 2012). Hare & Gardner (1985) plotted the elevations of the Cerro Azul erosional surface that caps the interior mountains that run along the Nicoya Peninsula to first determine trench-parallel uplift trends [Figure 26]. This map-based study was followed by field-based research providing additional constraints on terrace uplift patterns (e.g. Marshall and Anderson, 1995; Fisher et al., 1998; Gardner et al., 2001). Marshall et al. (2008, 2010, 2012) mapped and surveyed marine terraces along the entire Nicoya coastline to calculate uplift rates at discrete study sites [Figure 8]. More recently, Morrish (2015) performed a similar analysis to characterize uplift, using aggradational fluvial terraces within the interior mountains that run the length of the Nicoya Peninsula [Figure 27].

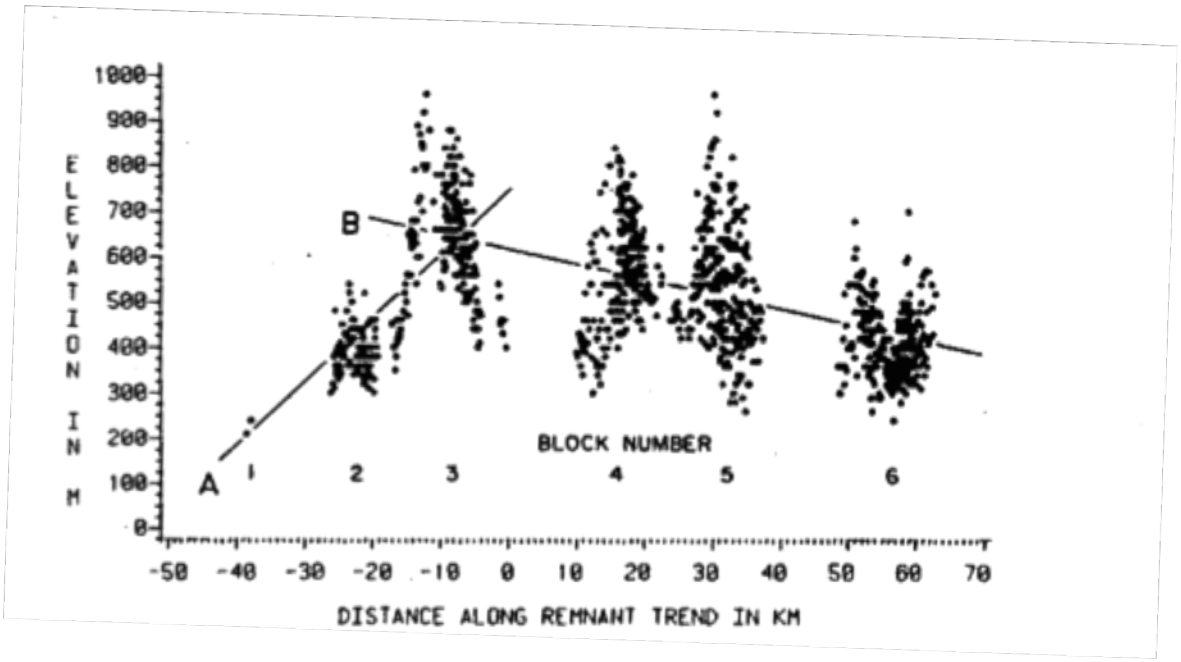

Figure 26: Scatter plot of elevation versus distance parallel to the remnant trend of the high elevation Cerro Azul surface (123.8º) with the regression lines shown. [A: ELEV = 741.82 + 13.88(T1); B: ELEV = 619.67-3.33(T1); T1 is the distance along the remnant trend] (Hare and Gardner, 1985).

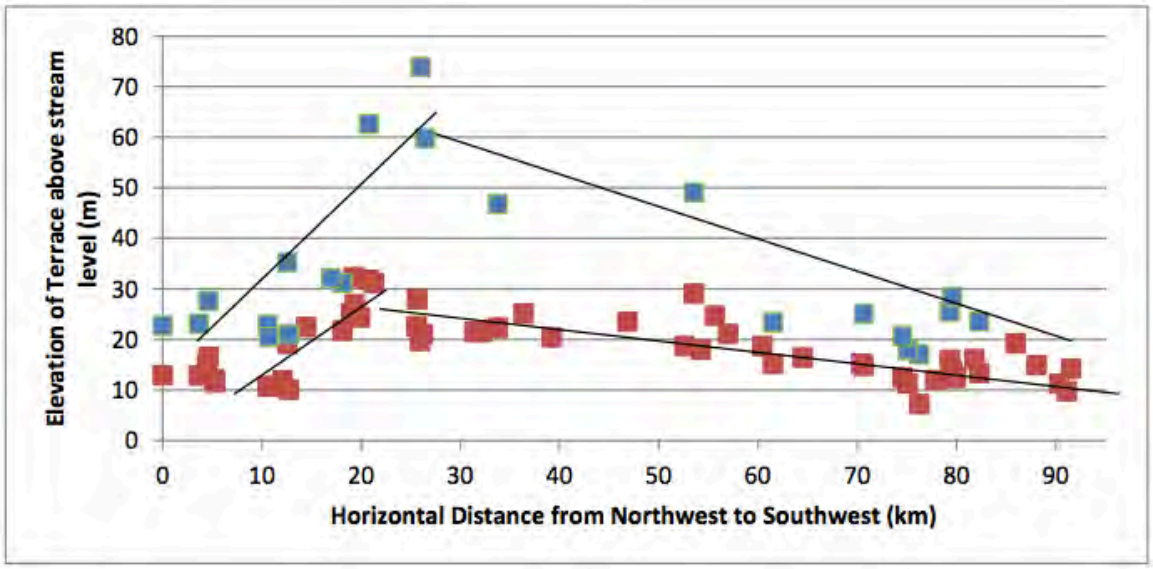

Figure 27: Scatter plot of Fluvial Terrace Height (FTH) versus trench-parallel (130º) distance along the length of the Nicoya Peninsula. FTH values are shown for two sets of fluvial terraces. Terrace locations are based on projection of terrace centroid points onto the projection line (Morrish, 2015).

Using the corrected DEM extracted inner-edge values, a similar plot of elevation versus distance parallel to the Middle America Trench was generated for this project [Figure 28]. A total of 460 elevation points were picked from the extracted terrace map [Figure 25] and used to create the new plot. The elevation points within the plot were split into three segments [Figure 28, Figure 29]. The first plot [Figure 28] splits up the three segments according to the mapped location of each of the three Cocos plate seafloor domains (EPR, CNS-1, CNS-2). The second plot [Figure 29] moves the segment boundary between the EPR and CNS-1 crust types to a location further northwest, representing the topographic and seismologic break across the peninsula recognized by Marshall et al. (2010). Linear trend-lines showing the overall uplift trend across the EPR and CNS-1 segments were also calculated [Figure 28, Figure 29].

Despite the inconsistency with the EPR/CNS-1 boundary mapped by Barckhausen (2001), Figure 29 more consistently matches previous field studies (e.g. Hare & Gardner, 1985; Marshall et al., 2008, 2010, 2012; Morrish, 2015), both in terms of the location of the morphotectonic segmentation and in terms of overall uplift trend. Figure 28, with the traditional boundary, has a decreasing elevation trend as you approach the boundary from the south, which is inconsistent with marine terrace ages and field data (Marshall et al., 2010). Moving the upper-plate deformation boundary, caused by the EPR/CNS-1 subduction, further north [Figure 29] allows a more reasonable elevation trend that supports the age data, with elevation values that peak at the boundary.

The Cobano surface at the southernmost end of the Nicoya Peninsula is well expressed in the plot of elevation versus distance [Figure 28, Figure 29], with at least three distinct elevation clusters showing terrace locations. Differentiation between the

Qt1 and Qt2 terraces of the Samara surface becomes more difficult as one moves further north along the coastline [Figure 30].

Elevation points were then converted to uplift values using the correction factors in Table 1 and age correlations from Marshall et al. (2008, 2010, 2012) [Appendix B]. Using the range of calculated elevation values, the range of ages corresponding to sea level highs (Marshall et al., 2010), and the ranges for paleo-sea level (Marshall et. al., 2010), two lines of uplift values were plotted, showing the range of potential uplift rates [Figure 31].

Most of the Peninsula has uplift rates around 0.3 m/ky, while the southernmost tip of the peninsula has uplift rates around 1-2 m/ky. A noticeable high anomaly in uplift rates occurs from the 60-80 km distance along the coastline. One possibility is that uplift is actually 2-3 times higher at that location, due to the boundary between the EPR and CNS-1 crust types. Another possible interpretation is that the anomalously high uplift rates are an artifact of incorrect terrace age correlations; the presence of higher and older terraces (e.g. OIS 7) along this stretch of the Nicoya Peninsula could cause such an anomaly.

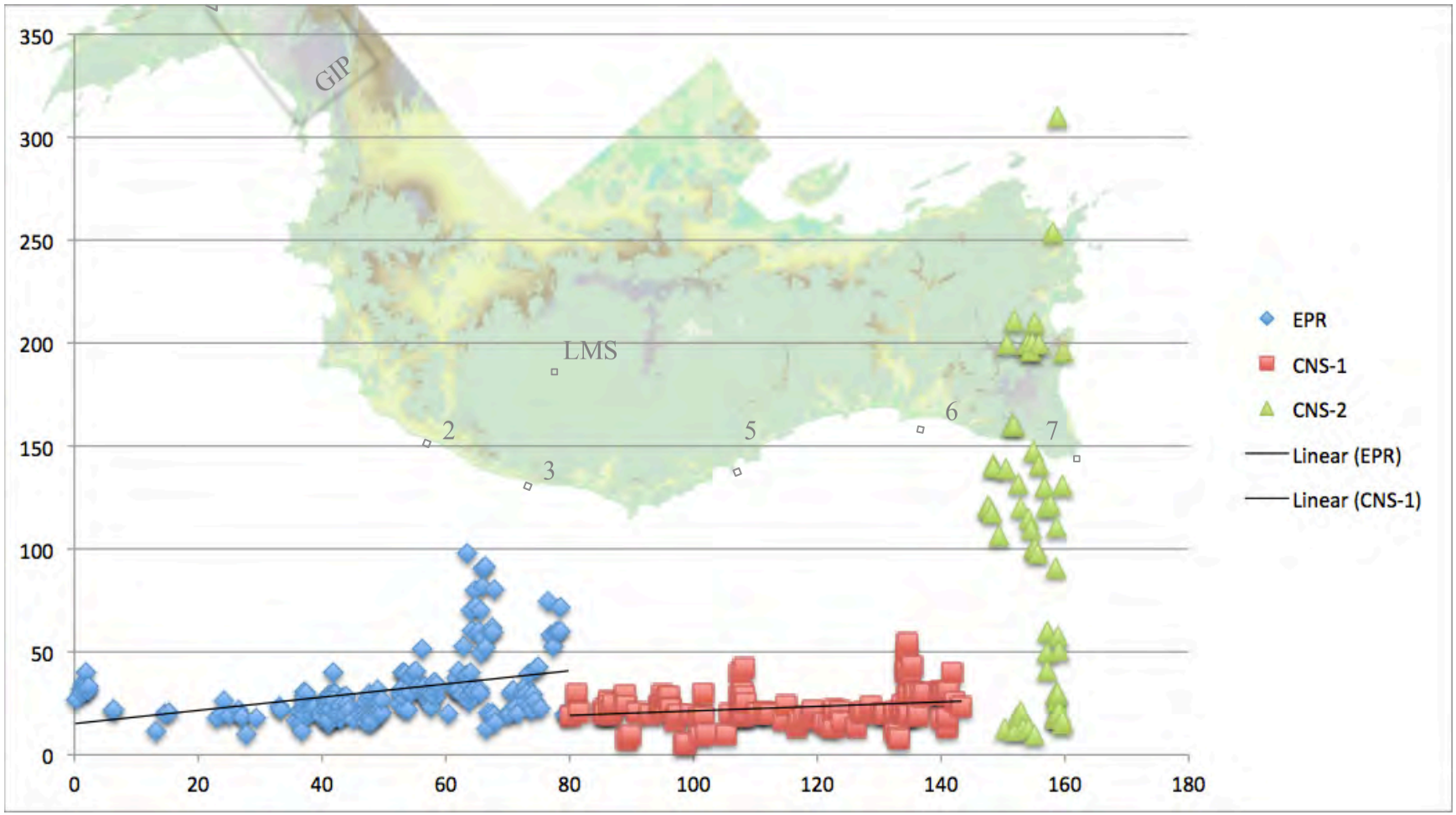

Figure 28: Scatter plot of Estimated Inner Edge Elevation versus coast parallel (130º) distance (from northwest to southeast) along the length of the Nicoya Peninsula. The trendline to the north of the traditional EPR/CNS-1 boundary (Barckhausen et al., 2001) is Y= 0.3211x + 15.149. The trendline in the middle of the peninsula, to the south of the EPR/CNS-1 boundary is Y= 0.1091x + 10.425. In the south, where the CNS-2 plate subducts, at least three distinct terraces can be seen.

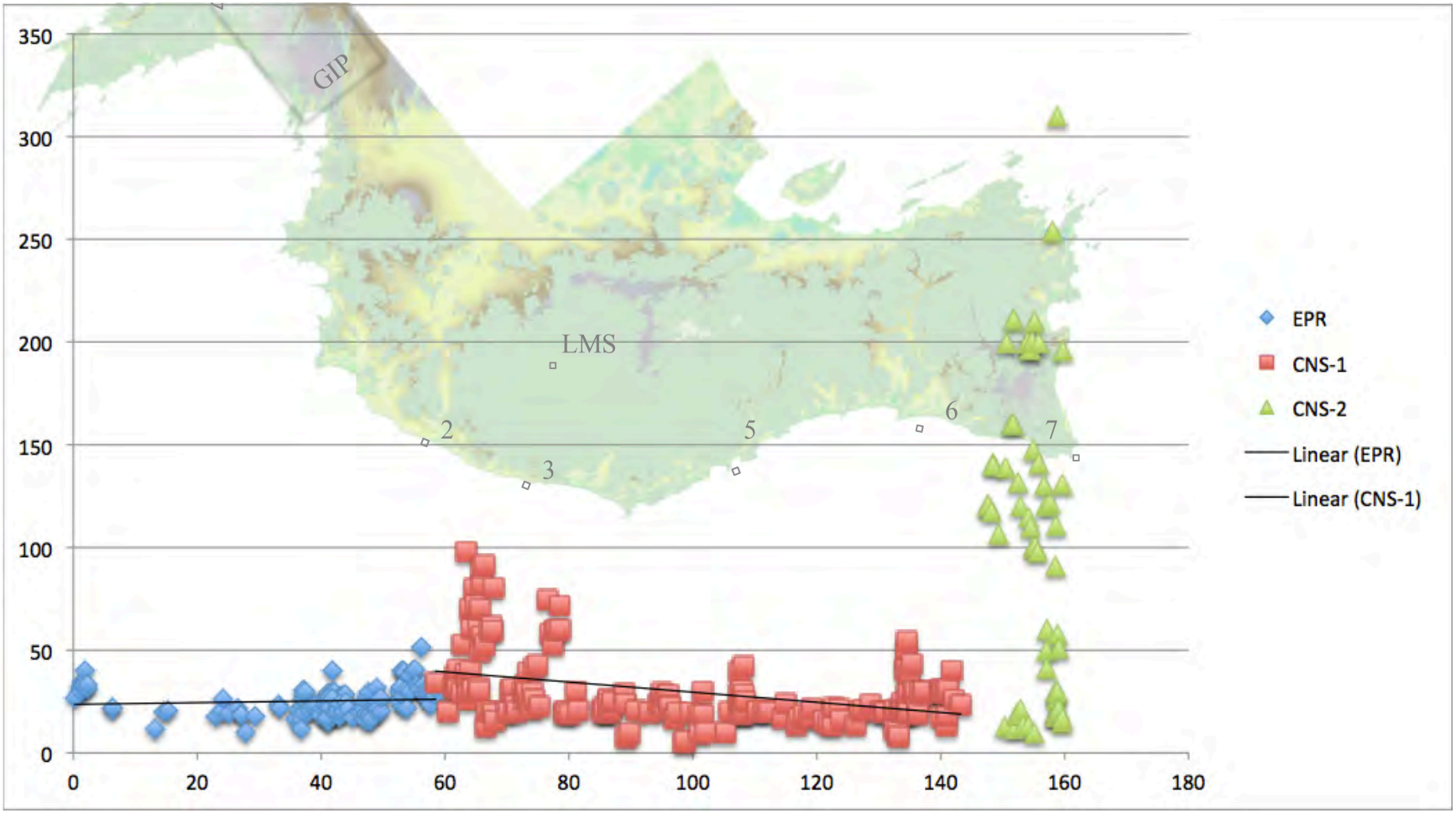

Figure 29: Scatter plot of Estimated Inner Edge Elevation (meters) versus coast parallel (130º) distance (kilometers; from northwest to southeast) along the length of the Nicoya Peninsula. The trendline to the north of the break in topography and seismicity (Newman et al., 2002; recognized in Marshall et al., 2010) on the Nicoya Peninsula is Y= 0.0423x + 23.619. The trendline in the middle of the peninsula, to the south of the EPR/CNS-1 boundary is Y= -0.2469x + 54.27. In the south, where the CNS-2 plate subducts, at least three distinct terraces can be seen.

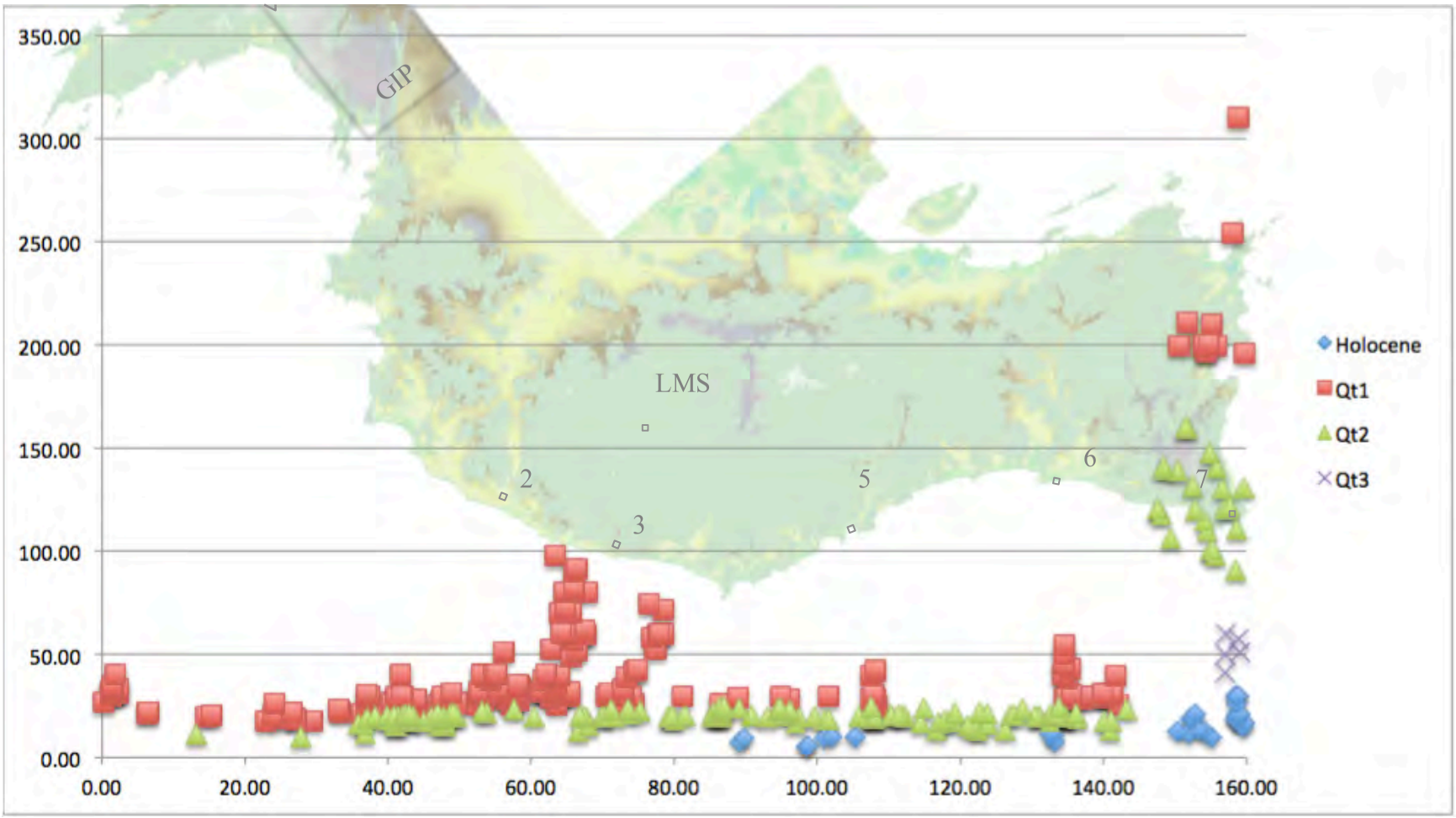

Figure 30: Elevation (m) versus Distance (km) of coastal terrace surfaces along the Nicoya Peninsula. The elevation points are sorted by potential age (terrace level) to allow further conversion to uplift data.

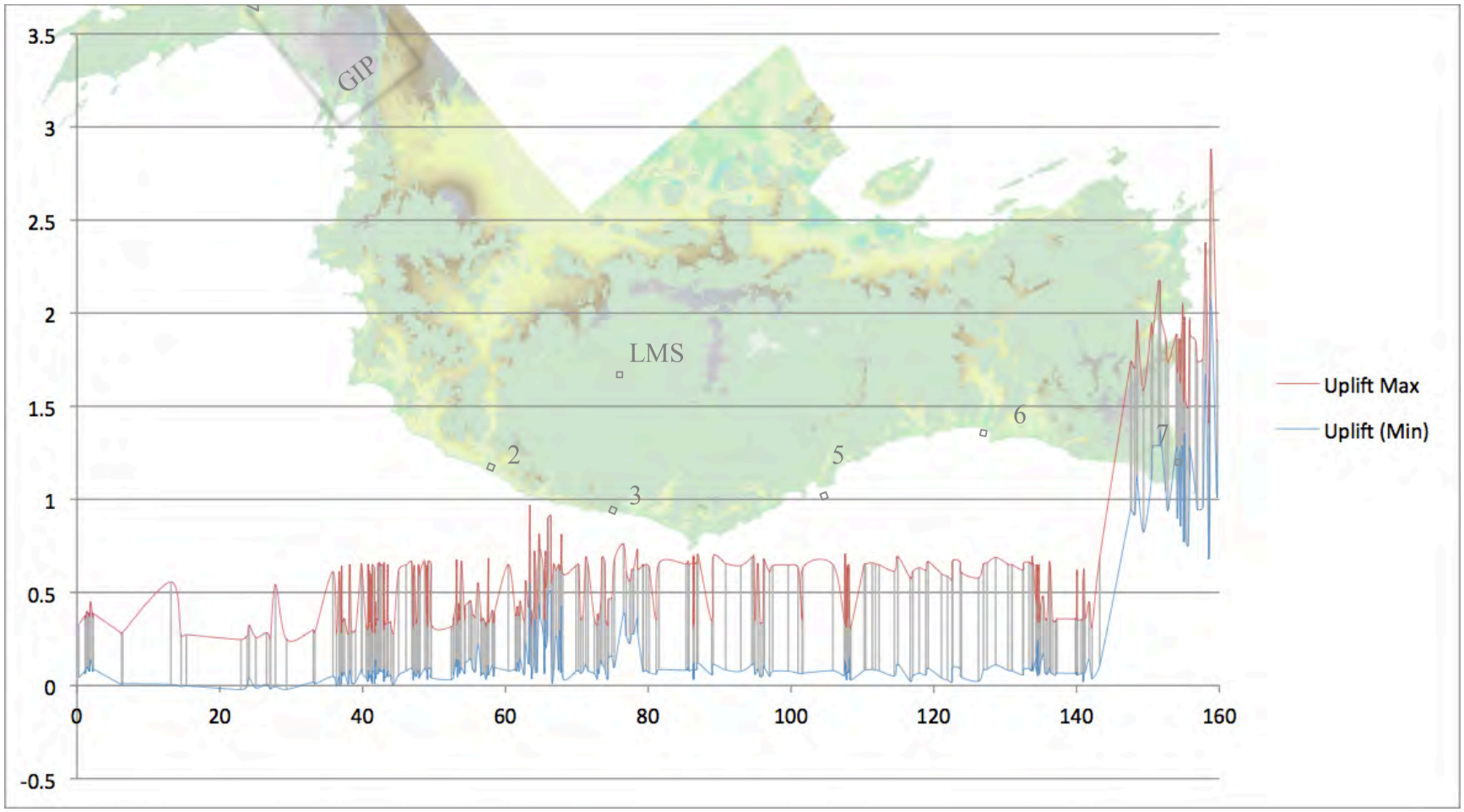

Figure 31: Uplift (m/ky) versus distance (km) across the Nicoya Peninsula. A subtle shift in uplift data is present around 60km, potentially showing the segmentation between the EPR and CNS-1 crust types. A much bigger jump in uplift data is present at 140km, showing the segmentation between the CNS-1 and CNS-2 crust types.

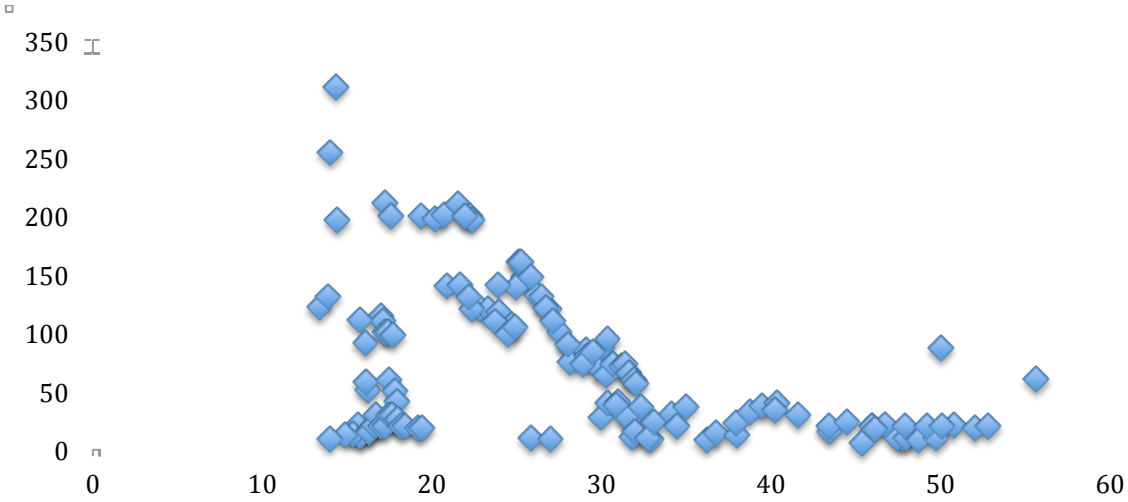

Figure 32: Scatter plot of Estimate Inner Edge Elevation (meters) versus coast parallel (40º) distance (kilometers; from southwest to northeast) along the southern edge of the Nicoya Peninsula [Figure 25].

A cross section of the terrace elevations along Site #7, consisting of the Cobano and Cabuya surfaces, was also created [Figure 32], showing the change in terrace elevation as one moves west to east along the bottom of the Nicoya Peninsula. Terrace elevations peak along the southwestern tip of the Nicoya Peninsula and plunge quickly as one moves eastward.

CONCLUSIONS

There were two initial goals of this research project: 1) to test a GIS methodology for mapping marine terraces in a region with site specific field data (Nicoya Peninsula, Costa Rica), and 2) to utilize the results in calculating and interpreting tectonic uplift rates..

To accomplish these goals, an existing GIS method (Scott and Pinter, 2003) was modified to identify and extract low-relief landscape surfaces (e.g., marine terraces) using Digital Terrain Models (DTM) constructed in ArcGIS software. The terrace extraction method uses slope, relief, and elevation DTMs to select cells that have values typical of gently sloping marine terraces, while avoiding false positive values that may be associated with other surfaces, like ridge tops and stream beds.

The terrace extraction procedure was modified in this study to work with a smaller cell size, and was calibrated to locate uplifted marine terraces along the coastlines of the Nicoya Peninsula, Costa Rica. The original methodology of Scott and Pinter (2003) was used to study marine terraces on Santa Cruz Island, California. In their study, the entire project area was mapped on 30-meter resolution USGS DEMs, which predetermined the 30-meter cell size and allowed for calibration of the methodology in an area that had been mapped completely in the field. The principal challenge in adapting their method for this project was to determine whether or not a limited sample of localized field sites could be successfully extrapolated over a larger area using the same approach. A smaller cell size of 12.5 meters was selected for use with the Costa Rica 1:25,000 scale Terra Project digital topographic data covering the Nicoya Peninsula. Five previously mapped field areas were used as source data to determine the best

combination of input values for the Nicoya Peninsula. Based on iterative testing, the optimum input values were determined (slope ≤15º, relief ≤15m within a radius of 87.5m, elevation ≥ 0m) and the terrace extraction procedure was extrapolated across the entire Nicoya Peninsula. Elevation correction values of 0.2-0.8 meters were within the error of ±2 meters that was expected for a topographic map with 10-meter contour lines. This study confirmed that this methodology could indeed be extrapolated over larger areas extending field mapping from site-specific locations into other unmapped areas along the coastline.

Once the methodology was proven successful, the second purpose of this project was to extract terrace inner edge elevations and convert those into tectonic uplift rates along the Nicoya Peninsula coastline. Elevation values were extracted and segmented two different ways: first according to offshore boundaries between the EPR, CNS-1, and CNS-2 crustal types (Barckhausen, 2001), and then according to major geomorphic boundaries seen on the peninsula (e.g., Hare and Gardner, 1985; Marshall et al., 2012). Terrace elevations were combined with isotopic age data, and correlated with sea level high stands to calculate uplift rates. These calculations were based on DTM extracted terrace elevations (calibrated by an elevation correction factor), and terrace geochronologic data (CRN, OSL, ^{14}C) from Marshall et al (2008, 2010, 2012). The resulting uplift rates help constrain the pattern of tectonic deformation in a more continuous manner along the margin-parallel length of the Nicoya Peninsula, filling in values between the prior localized field sites. A subtle shift in uplift rates (~0-0.5 m/ka to ~0.2-0.7 m/ka) is observed along the central Nicoya coast near the transition from EPR to

CNS-1 crust on the subducting Cocos plate, whereas a large jump in uplift rates (up to 1.5-2.5m/ka) occurs at the CNS-1/CNS-2 boundary near the peninsula's southern tip.

The modeled uplift pattern suggests that active tectonic deformation on the Nicoya Peninsula is driven by differences in the characteristics of the subducting slab beneath the peninsula (e.g., dip angle, roughness, thermal state, fluid flow, etc.). This project also confirms the prior observation (Marshall et al., 2010) that the break in upper plate deformation along the central Nicoya coast occurs ~30 km north of the offshore mapped trace of the EPR-CNS-1 boundary (Barckhausen, 2001). This could occur for several reasons: 1) the underlying crustal boundaries may actually be offset 30 km on the portion of the subducting plate currently underneath the peninsula, or 2) surface deformation patterns may be diffuse due to the thickness of crust between the upper plate and underlying subducting plate at depth. The sharp jump in uplift rates inboard of the CNS-1/CNS-2 boundary at the peninsula's southern tip is consistent with previous studies showing the impact of CNS-2 seamounts on this area (e.g., Marshall and Anderson, 1995; Gardner et al., 2001), with highest uplift rates at the tip, and terrace surfaces plunging downward quickly as you move further east, due to tilting of the associated geomorphic block. Further fieldwork is necessary to verify uplift trends modeled in this study for areas not previously mapped in the field.

FUTURE WORK

While the terrace extraction process described in this paper successfully extracted a number of surfaces across the Nicoya Peninsula, all previously unmapped or unidentified features found using this process should be verified, either through additional fieldwork or careful evaluation of aerial photographs. The DTM method successfully extracted a range of terrace-like geomorphic surfaces, however their geomorphic nature cannot be defined using digital data alone. Therefore, some of the extracted surfaces may not be marine terraces, but rather features like fluvial terraces or volcanic features like the ignimbrite flow recognized in this study. Further field verification of all features will be necessary to characterize their geomorphic origin. Great care should be taken when creating new field maps to not only denote marine terraces, but also fluvial terraces, flood plains, and modern coastal lowlands (e.g. beaches, wetlands).

An additional complication of a tectonically complex study area like the Nicoya Peninsula is that terrace surfaces are not uniform over distance, and therefore can not simply be sorted by elevation to determine which terrace was extracted. A more easily interpreted test of this terrace extraction method might be one limited to an area with more consistent uplift rates and uniform terrace elevations.

REFERENCES

Anderson, R. S., and Anderson, S. P., 2010, Geomorphology: the mechanics and chemistry of landscapes: New York, Cambridge University Press, ___ p.

Anderson, R.S., Densmore, A.L., and Ellis, M.A., 1999, The generation and degradation of marine terraces: Blackwell Science Ltd., Basin Research v. 11, p. 7-19.

Barckhausen, U., Ranero, C.R., von Huene, R., Cande, S.C., and Roeser, H.A., 2001, Revised tectonic boundaries in the Cocos Plate off Costa Rica: Implications for the segmentation of the convergent margin and for plate tectonic models: Journal of Geophysical Research, v. 106, p. 19,207–19,220.

Baumgartner, P. O., Mora, C. R., Butterlin, J., Sigal, J., Glacon, G., Azema, J., and Bourgois, J., 1984, Sedimentación y paleogeografía del Cretócio y Cenozóico del litoral Pacífico de Costa Rica: Revista Geológica de América Central, v. 1, p. 57–136.

Bolstad, Paul, 2007, GIS Fundamentals: A First Text on Geographic Information Systems, 3rd Edition, Eider Press, 2005.

Bradley, W.C. and Griggs, G.B., 1976. Form, genesis, and deformation of central California wave-cut platforms, Geological Society of America Bulletin, v. 87.3, p. 433-449.

Dengo, G., 1962, Estudio geológico de la región de Guanacaste, Costa Rica, Instituto Geográfico de Costa Rica.

Denyer, P., Aguilar, T., and Montero, W., 2014, Cartografía geológica de la Península de Nicoya, Costa Rica: Editorial Universidad de Costa Rica, San José, 207 p.

DeMets, C., Gordon, R. G., and Argus, D. F., 2010, Geologically current plate motions: Geophysical Journal International, v. 181.1, p. 1-80.

Fisher, D.M., Gardner, T.W., Marshall, J.S., Sak, P.B. and Protti, M., 1998, Effect of subducting sea-floor roughness on fore-arc kinematics, Pacific coast, Costa Rica. Geology, v. 26.5, pp.467-470.

Florinsky, I.V., 1998, Combined analysis of digital terrain models and remotely sensed data in landscape investigations, Progress in Physical Geography v.22, p. 33-60.

Frye, Charlie, 2007, Choosing an appropriate cell size when interpolating raster data: https://blogs.esri.com/esri/arcgis/2007/07/03/choosing-an-appropriate-cell-size-when-interpolating-raster-data/ (Accessed April 15, 2016).

Gardner, T., Marshall, J., Merritts, D., Bee, B., Burgette, R., Burton, E., Cooke, J., Kehrwald, N., Protti, M., Fisher, D. and Sak, P., 2001, Holocene forearc block rotation in response to seamount subduction, southeastern Peninsula de Nicoya, Costa Rica, Geology, v. 29.2, p. 151-154.

Guth, P.L., 1995, Slope and aspect calculations on gridded digital elevation models: Examples from a geomorphometric toolbox for personal computers, Zeitschrift fur Geomorphologie Supplementband, p. 31-52.

Hare, P.W., and Gardner, T.W., 1985, Geomorphic indicators of vertical neotectonism along converging plate margins, Nicoya Peninsula, Costa Rica, *in* Morisawa, M., and Hack, J.T., eds., Tectonic geomorphology: Proceedings of the 15th Geomorphology Symposia Series, Binghamton, p. 76-104.

Hey, Richard, 1977, Tectonic evolution of the Cocos-Nazca spreading center: GSA Bulletin, v. 88, p. 1404-1420.

Ijjasz-Vasques, E.J. and Bras, R.L., 1995, Scaling regimes of local slope versus contributing area in digital elevation models, Geomorphology v. 12.4, p. 299-311.

LaFromboise, E.J., 2012, Neotectonism of the Nicoya Peninsula, Costa Rica: geomorphology and earthquake relocations along the Nicoya Seismic Gap (Doctoral dissertation, California State University, Northridge).

LaJoie, K.R., 1986, Coastal Tectonics, *in* Wallace, R.E., ed., Active Tectonics, Studies in Geophysics, Washington DC, National Academy Press, p. 95-124.

Lundberg, N., 1982, Evolution of the slope landward of the Middle America Trench, Nicoya Peninsula, Costa Rica, Geological Society, London, Special Publications, v. 10.1, p. 131-147.

Marshall, J.M., 2007, The Geomorphology and Physiographic Provinces of Central America, *in* Bundschuh, J., and Alvarado G.E., eds., Central America: Geology, Resources and Hazards, London, Taylor & Francis, p. 345-394.

Marshall, J.M. 2010-2012. Seismogenesis of the Middle America Trench at the Nicoya Peninsula over multiple seismic cycles. NSF Ocean Sciences – MARGINS Program: Award OCE 0948312 Final Project Report.

Marshall, J.S., LaFromboise, E.J., Utick, J.D., Khaw, F., Morrish, S.C., Piestrzeniewicz, P., Gardner, T.W., Protti, M. and Spotila, J.A., 2008, Tectonic geomorphology and paleoseismology of the Nicoya Peninsula seismogenic zone, Costa Rica, National Science Foundation MARGINS Program, The Next Decade of the Seismogenic Zone Experiment, p. 22-26.

Marshall, J.M., and Anderson R.S. 1995. Quaternary uplift and seismic cycle deformation, Peninsula de Nicoya, Costa Rica. GSA Bulletin, v.107.4, p. 463-473

Morrish, Shawn C. 2015. Characterization and digital morphotectonic analysis of drainage basins in a deforming forearc, Nicoya Peninsula, Costa Rica. Masters Thesis, California State Polytechnic University, Pomona.

Newman, A.V., Schwartz, S.Y., Gonzales, V., DeShon, H.R., Protti, J.M., and Dorman, L., 2002. Along strike variability in the seismogenic zone below Nicoya Peninsula, Costa Rica, Geophysical Research Letters, v. 29, doi:10.1029/2002GL015409.

Sak, P.B., Fisher, D.M., Gardner, T.W., Marshall, J.S. and LaFemina, P.C., 2009, Rough crust subduction, forearc kinematics, and Quaternary uplift rates, Costa Rican segment of the Middle American Trench, Geological Society of America Bulletin, v. 121.7-8, p. 992-1012.

Scott, A. T., & Pinter, N., 2003. Extraction of coastal terraces and shoreline-angle elevations from digital terrain models, Santa Cruz and Anacapa Islands, California. Physical Geography, v. 24.4, p. 271-294.

Sinton, C. W., Duncan, R. A., & Denyer, P., 1997. Nicoya Peninsula, Costa Rica: A single suite of Caribbean oceanic plateau magmas, Journal of Geophysical Research, v.102.B7, p. 15,507-15,520.

Tobler, Waldo. 1988. "Resolution, Resampling, and All That", pp. 129-137 of H. Mounsey and R. Tomlinson, eds., Building Data Bases for Global Science, London, Taylor and Francis.

APPENDIX A

SUCCESS DATA

COMBINED NICOYA PENINSULA

Table 2: Raw Success Data

Slope	Radius	Range	0	1	2	3	4	5	6	7
5	25	5	687269	145010	107219	152410	24491	74352	5854	17662
5	25	10	680760	151519	102594	157035	24335	74508	5751	17765
5	25	15	680119	152160	101883	157746	24335	74508	5748	17768
5	25	20	680020	152259	101844	157785	24335	74508	5748	17768
5	25	25	680004	152275	101842	157787	24335	74508	5748	17768
5	37	5	721135	111144	128514	131115	28194	70649	7884	15632
5	37	10	687686	144593	106570	153059	24422	74421	5863	17653
5	37	15	681560	150719	102786	156843	24339	74504	5751	17765
5	37	20	680364	151915	102021	157608	24335	74508	5750	17766
5	37	25	680088	152191	101872	157757	24335	74508	5748	17768
5	50	5	746113	86166	149840	109789	32132	66711	10327	13189
5	50	10	701577	130702	113878	145751	25207	73636	6633	16883
5	50	15	686778	145501	104552	155077	24478	74365	5867	17649
5	50	20	682145	150134	102453	157176	24359	74484	5763	17753
5	50	25	680563	151716	101940	157689	24342	74501	5751	17765
5	62	5	767385	64894	171202	88427	36361	62482	13166	10350
5	62	10	722757	109522	129418	130211	27362	71481	8458	15058
5	62	15	699914	132365	111598	148031	25307	73536	6600	16916
5	62	20	689488	142791	105755	153874	24578	74265	5951	17565
5	62	25	684168	148111	103195	156434	24398	74445	5802	17714
5	75	5	779757	52522	184807	74822	39365	59478	14954	8562
5	75	10	737188	95091	141416	118213	29284	69559	9982	13534
5	75	15	711145	121134	118704	140925	26328	72515	7686	15830
5	75	20	697246	135033	109787	149842	25135	73708	6341	17175
5	75	25	689055	143224	105017	154612	24617	74226	5965	17551
10	25	5	666787	165492	91694	167935	23055	75788	5005	18511
10	25	10	591482	240797	60633	198996	19229	79614	3166	20350
10	25	15	586989	245290	57280	202349	19208	79635	3151	20365
10	25	20	586567	245712	56993	202636	19208	79635	3151	20365
10	25	25	586503	245776	56974	202655	19208	79635	3151	20365

Slope	Radius	Range	0	1	2	3	4	5	6	7
10	37	5	720673	111606	127954	131675	28180	70663	7853	15663
10	37	10	645370	186909	78872	180757	21172	77671	4417	19099
10	37	15	598119	234160	61166	198463	19363	79480	3237	20279
10	37	20	588548	243731	57913	201716	19213	79630	3156	20360
10	37	25	586878	245401	57142	202487	19208	79635	3152	20364
10	50	5	746007	86272	149783	109846	32128	66715	10318	13198
10	50	10	687014	145265	101574	158055	23687	75156	6065	17451
10	50	15	632080	200199	70834	188795	20697	78146	4085	19431
10	50	20	601551	230728	60672	198957	19444	79399	3292	20224
10	50	25	590534	241745	57695	201934	19248	79595	3171	20345
10	62	5	767333	64946	171195	88434	36361	62482	13164	10352
10	62	10	719019	113260	125629	134000	26552	72291	8195	15321
10	62	15	671000	161279	88263	171366	22861	75982	5654	17862
10	62	20	635597	196682	71688	187941	20756	78087	4034	19482
10	62	25	609887	222392	62505	197124	19646	79197	3450	20066
10	75	5	779714	52565	184805	74824	39365	59478	14954	8562
10	75	10	735677	96602	139837	119792	28698	70145	9805	13711
10	75	15	692492	139787	101607	158022	24428	74415	7074	16442
10	75	20	659419	172860	82071	177558	22098	76745	4866	18650
10	75	25	630190	202089	68386	191243	20440	78403	3948	19568
15	25	5	666596	165683	91356	168273	23055	75788	5005	18511
15	25	10	552167	280112	46766	212863	17657	81186	2548	20968
15	25	15	502979	329300	34817	224812	16662	82181	2039	21477
15	25	20	501006	331273	33631	225998	16662	82181	2037	21479
15	25	25	500805	331474	33521	226108	16662	82181	2037	21479
15	37	5	720671	111608	127954	131675	28180	70663	7853	15663
15	37	10	644468	187811	77529	182100	20936	77907	4342	19174
15	37	15	565021	267258	46575	213054	17976	80867	2663	20853
15	37	20	515097	317182	36685	222944	16752	82091	2103	21413
15	37	25	502632	329647	34108	225521	16665	82178	2040	21476
15	50	5	746006	86273	149783	109846	32128	66715	10318	13198
15	50	10	686795	145484	101329	158300	23530	75313	6024	17492
15	50	15	621467	210812	62970	196659	19925	78918	3816	19700
15	50	20	565839	266440	45634	213995	17799	81044	2614	20902
15	50	25	525269	307010	36856	222773	16872	81971	2187	21329
15	62	5	767333	64946	171195	88434	36361	62482	13164	10352
15	62	10	718872	113407	125457	134172	26430	72413	8166	15350
15	62	15	666427	165852	83472	176157	22339	76504	5491	18025

Slope	Radius	Range	0	1	2	3	4	5	6	7
15	62	20	620661	211618	61893	197736	19695	79148	3565	19951
15	62	25	574851	257428	46241	213388	17868	80975	2754	20762
15	75	5	779714	52565	184805	74824	39365	59478	14954	8562
15	75	10	735552	96727	139697	119932	28596	70247	9778	13738
15	75	15	689604	142675	98196	161433	23993	74850	6948	16568
15	75	20	650246	182033	74582	185047	21221	77622	4487	19029
15	75	25	607624	224655	55107	204522	18994	79849	3354	20162
5	87	5	793135	43370	195460	64169	42519	56324	16546	7136
5	87	10	753094	83411	152320	107309	31284	67559	11484	12198
5	87	15	725969	110536	126817	132812	27402	71441	9076	14606
5	87	20	709425	127080	114929	144700	25925	72918	7075	16607
5	87	25	698853	137652	107714	151915	25009	73834	6405	17277
5	100	5	801019	35486	205593	54036	46507	52336	17900	5782
5	100	10	763923	72582	162511	97118	33535	65308	12877	10805
5	100	15	737011	99494	136281	123348	28616	70227	10451	13231
5	100	20	719130	117375	121685	137944	26866	71977	8006	15676
5	100	25	706322	130183	111895	147734	25630	73213	6909	16773
5	112	5	806879	29626	214532	45097	51000	47843	18958	4724
5	112	10	773252	63253	171167	88462	35698	63145	14194	9488
5	112	15	745982	90523	145026	114603	29737	69106	11755	11927
5	112	20	728286	108219	128995	130634	27869	70974	9030	14652
5	112	25	713800	122705	116883	142746	26332	72511	7593	16089
5	125	5	811745	24760	221589	38040	55234	43609	19911	3771
5	125	10	781252	55253	179455	80174	37961	60882	15423	8259
5	125	15	753447	83058	152456	107173	30889	67954	13030	10652
5	125	20	736627	99878	136887	122742	28824	70019	10102	13580
5	125	25	721213	115292	122466	137163	27141	71702	8393	15289
5	137	5	815370	21135	226712	32917	58051	40792	20636	3046
5	137	10	787214	49291	185866	73763	39939	58904	16369	7313
5	137	15	758965	77540	157941	101688	31955	66888	14048	9634
5	137	20	742717	93788	143105	116524	29554	69289	10999	12683
5	137	25	727359	109146	127491	132138	27826	71017	9114	14568
5	150	5	818541	17964	231151	28478	60659	38184	21251	2431
5	150	10	792561	43944	192099	67530	41850	56993	17208	6474
5	150	15	764081	72424	162903	96726	33013	65830	15033	8649
5	150	20	747949	88556	148369	111260	30277	68566	11862	11820
5	150	25	732849	103656	132626	127003	28462	70381	9844	13838
10	87	5	793098	43407	195460	64169	42519	56324	16546	7136

Slope	Radius	Range	0	1	2	3	4	5	6	7
10	87	10	752138	84367	151403	108226	30774	68069	11334	12348
10	87	15	712958	123547	114157	145472	25819	73024	8617	15065
10	87	20	681785	154720	92757	166872	23385	75458	5917	17765
10	87	25	652456	184049	75547	184082	21420	77423	4663	19019
10	100	5	800982	35523	205593	54036	46507	52336	17900	5782
10	100	10	763174	73331	161827	97802	33095	65748	12744	10938
10	100	15	727803	108702	127239	132390	27225	71618	10077	13605
10	100	20	699314	137191	104188	155441	24729	74114	7095	16587
10	100	25	670785	165720	84633	174996	22561	76282	5461	18221
10	112	5	806845	29660	214532	45097	51000	47843	18958	4724
10	112	10	772634	63871	170588	89041	35314	63529	14083	9599
10	112	15	739059	97446	138343	121286	28483	70360	11436	12246
10	112	20	713287	123218	115201	144428	25961	72882	8298	15384
10	112	25	686121	150384	93840	165789	23664	75179	6354	17328
10	125	5	811714	24791	221589	38040	55234	43609	19911	3771
10	125	10	780706	55799	178985	80644	37633	61210	15322	8360
10	125	15	747891	88614	147369	112260	29728	69115	12757	10925
10	125	20	725013	111492	126149	133480	27052	71791	9508	14174
10	125	25	699378	137127	103217	156412	24841	74002	7356	16326
10	137	5	815346	21159	226712	32917	58051	40792	20636	3046
10	137	10	786722	49783	185464	74165	39645	59198	16275	7407
10	137	15	754243	82262	153780	105849	30890	67953	13809	9873
10	137	20	733044	103461	134326	125303	27894	70949	10477	13205
10	137	25	708873	127632	110900	148729	25657	73186	8216	15466
10	150	5	818523	17982	231151	28478	60659	38184	21251	2431
10	150	10	792113	44392	191754	67875	41582	57261	17131	6551
10	150	15	759917	76588	159460	100169	32053	66790	14839	8843
10	150	20	739706	96799	141127	118502	28715	70128	11393	12289
10	150	25	717041	119464	118305	141324	26376	72467	9079	14603
15	87	5	793098	43407	195460	64169	42519	56324	16546	7136
15	87	10	752031	84474	151286	108343	30681	68162	11309	12373
15	87	15	710923	125582	111595	148034	25439	73404	8515	15167
15	87	20	675441	161064	86873	172756	22637	76206	5597	18085
15	87	25	636615	199890	64420	195209	20146	78697	4147	19535
15	100	5	800982	35523	205593	54036	46507	52336	17900	5782
15	100	10	763079	73426	161723	97906	33009	65834	12721	10961
15	100	15	726357	110148	125391	134238	26890	71953	9997	13685
15	100	20	694818	141687	99696	159933	24069	74774	6812	16870

Slope	Radius	Range	0	1	2	3	4	5	6	7
15	100	25	659541	176964	75536	184093	21485	77358	5007	18675
15	112	5	806845	29660	214532	45097	51000	47843	18958	4724
15	112	10	772556	63949	170497	89132	35234	63609	14064	9618
15	112	15	737937	98568	136964	122665	28204	70639	11371	12311
15	112	20	709991	126514	111739	147890	25352	73491	8041	15641
15	112	25	677878	158627	86452	173177	22741	76102	5955	17727
15	125	5	811714	24791	221589	38040	55234	43609	19911	3771
15	125	10	780635	55870	178900	80729	37564	61279	15304	8378
15	125	15	746956	89549	146315	113314	29491	69352	12709	10973
15	125	20	722455	114050	123429	136200	26505	72338	9274	14408
15	125	25	693157	143348	97273	162356	24015	74828	6994	16688
15	137	5	815346	21159	226712	32917	58051	40792	20636	3046
15	137	10	786657	49848	185386	74243	39584	59259	16258	7424
15	137	15	753413	83092	152943	106686	30673	68170	13776	9906
15	137	20	730910	105595	132116	127513	27395	71448	10260	13422
15	137	25	703849	132656	105922	153707	24863	73980	7884	15798
15	150	5	818523	17982	231151	28478	60659	38184	21251	2431
15	150	10	792056	44449	191690	67939	41530	57313	17115	6567
15	150	15	759158	77347	158770	100859	31845	66998	14815	8867
15	150	20	737882	98623	139284	120345	28245	70598	11191	12491
15	150	25	712824	123681	114135	145494	25618	73225	8780	14902

APPENDIX B

TRANSECT DATA

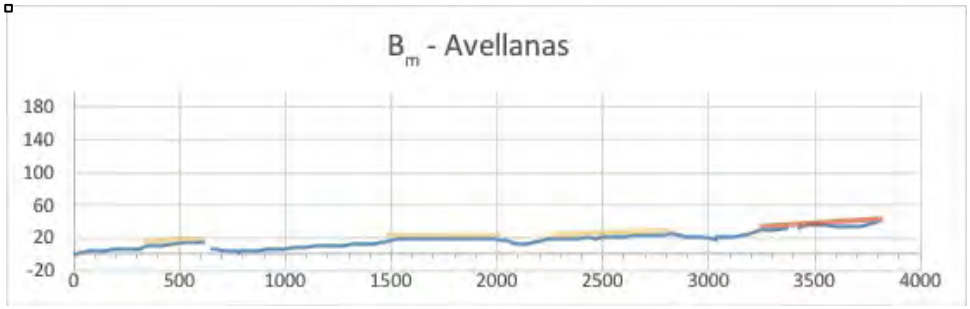

Figure 33: Transect B based on original field data. (Marshall et al., 2010)

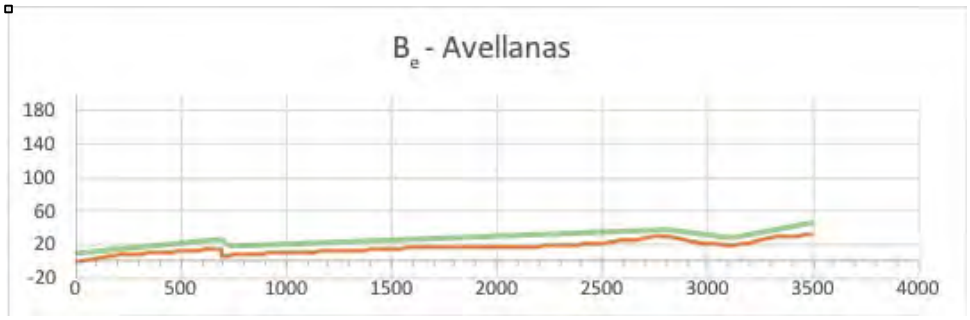

Figure 34: Transect B based on extracted terrace data.

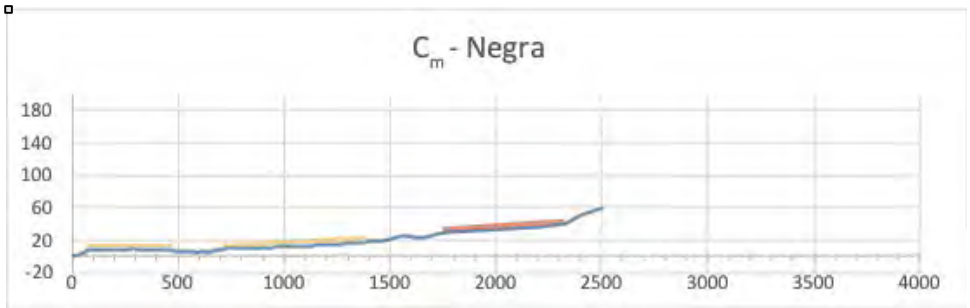

Figure 35: Transect C based on original field data. (Marshall et al., 2010)

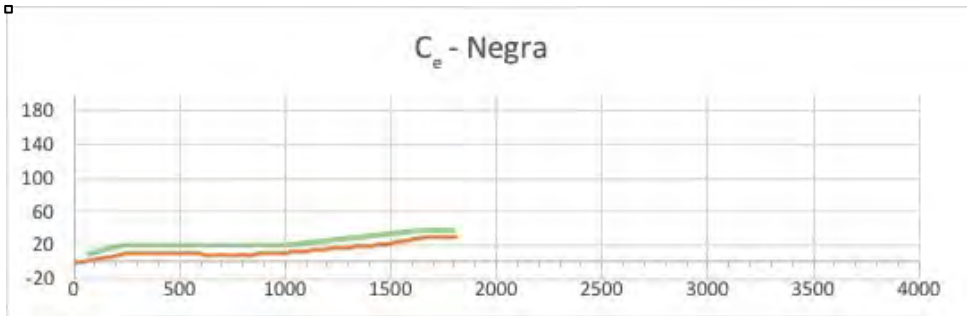

Figure 36: Transect C based on extracted terrace data.

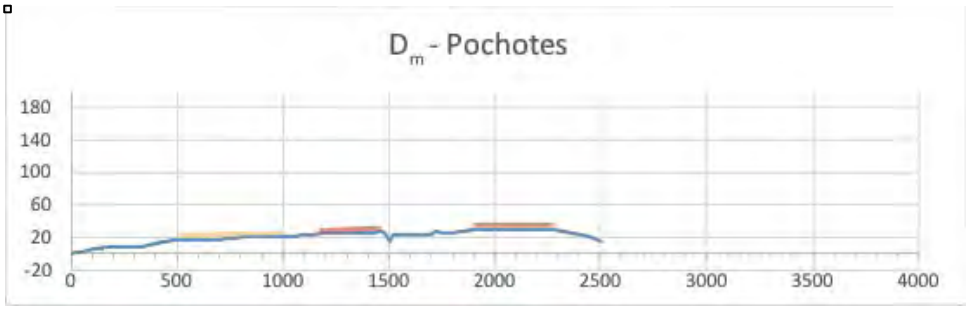

Figure 37: Transect D based on original field data. (Marshall et al., 2010)

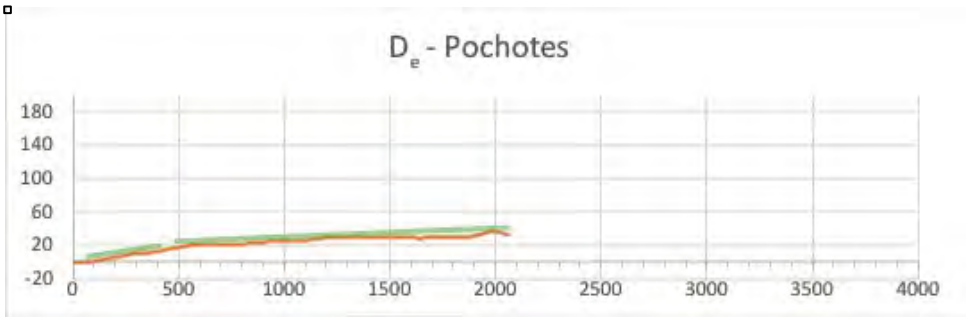

Figure 38: Transect D based on extracted terrace data.

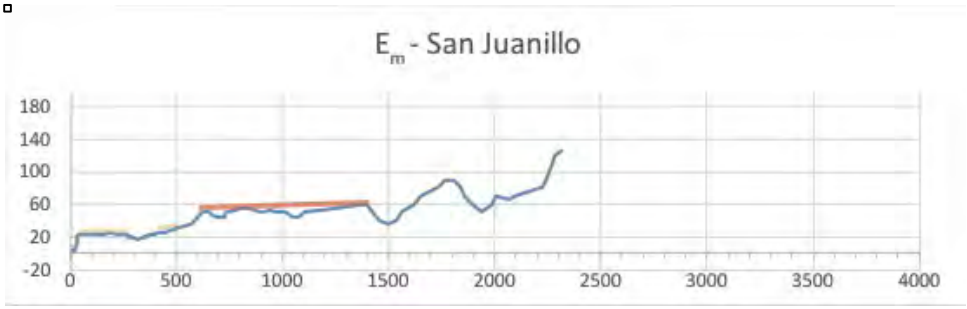

Figure 39: Transect E based on original field data. (Marshall et al., 2010)

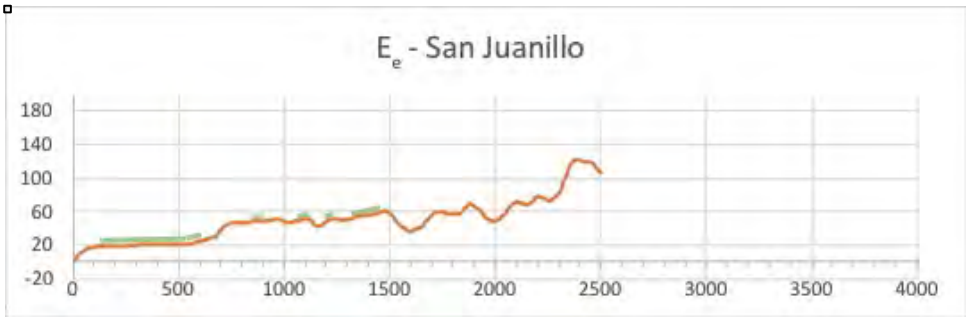

Figure 40: Transect E based on extracted terrace data.

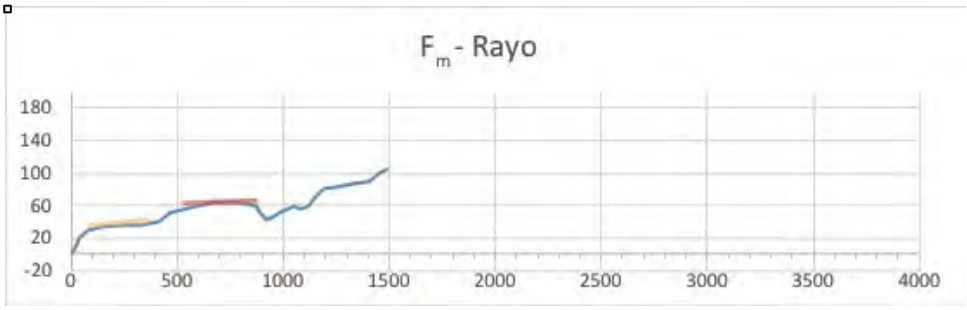

Figure 41: Transect F based on original field data. (Marshall et al., 2010)

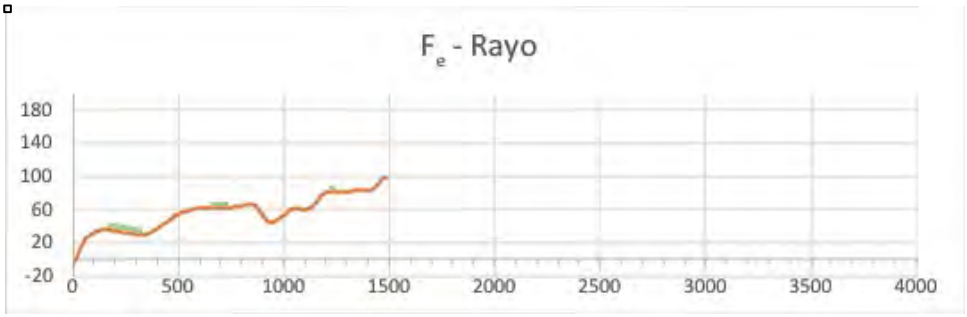

Figure 42: Transect F based on extracted terrace data.

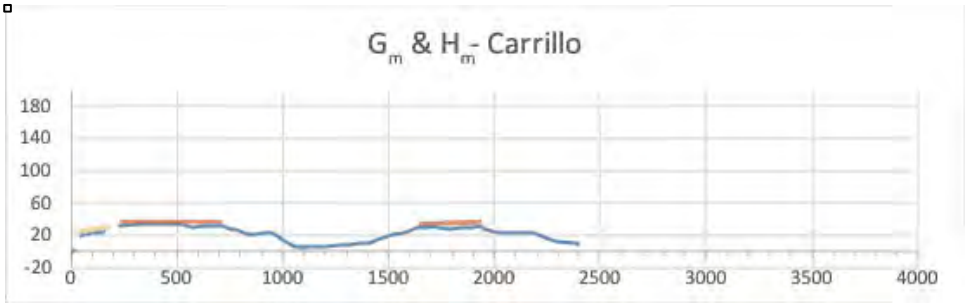

Figure 43: Transect G & H based on original field data. (Marshall et al., 2010)

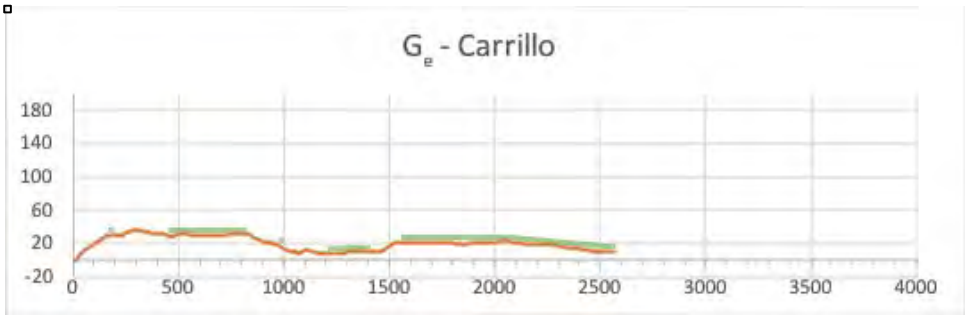

Figure 44: Transect G based on extracted terrace data.

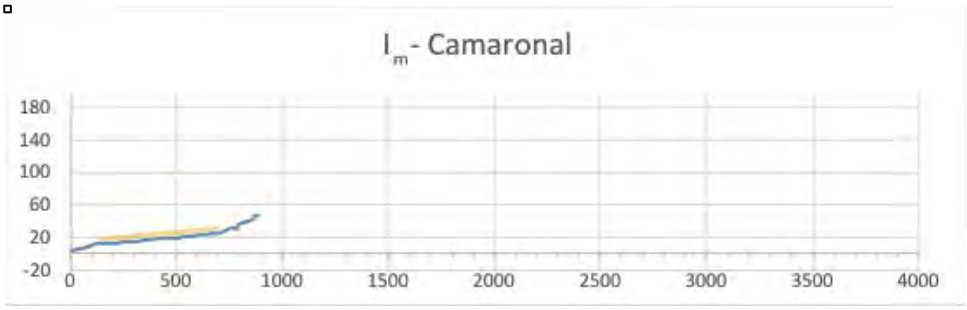

Figure 45: Transect I based on original field data. (Marshall et al., 2010)

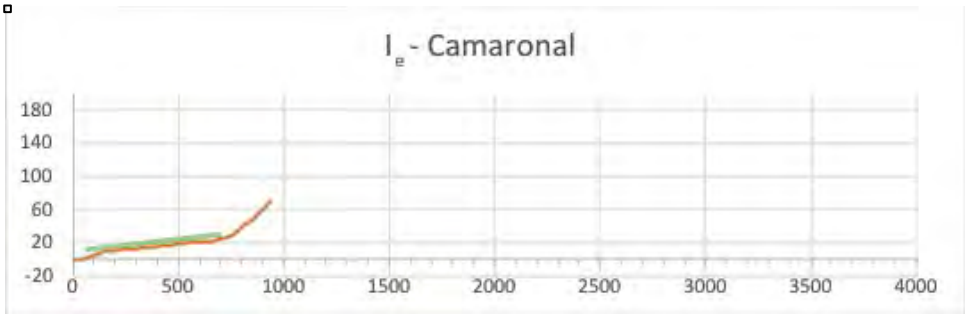

Figure 46: Transect I based on extracted terrace data.

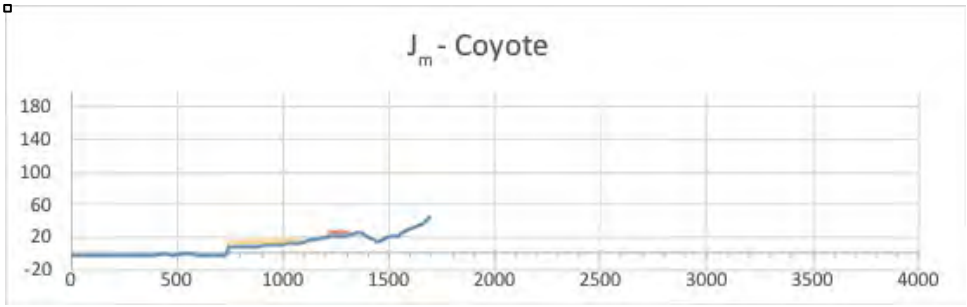

Figure 47: Transect J based on original field data. (Marshall et al., 2010)

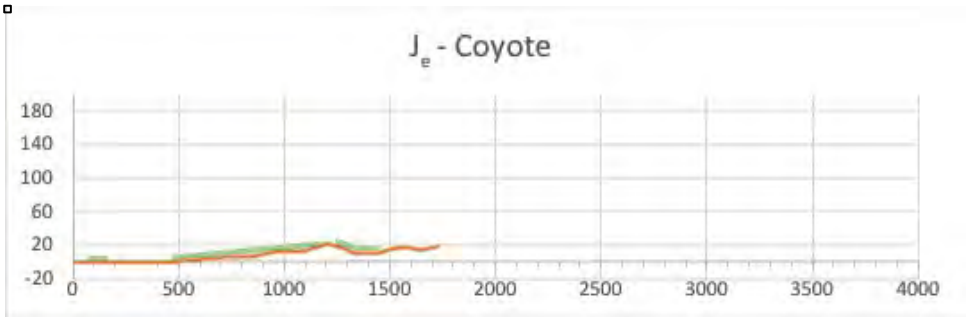

Figure 48: Transect J based on extracted terrace data.

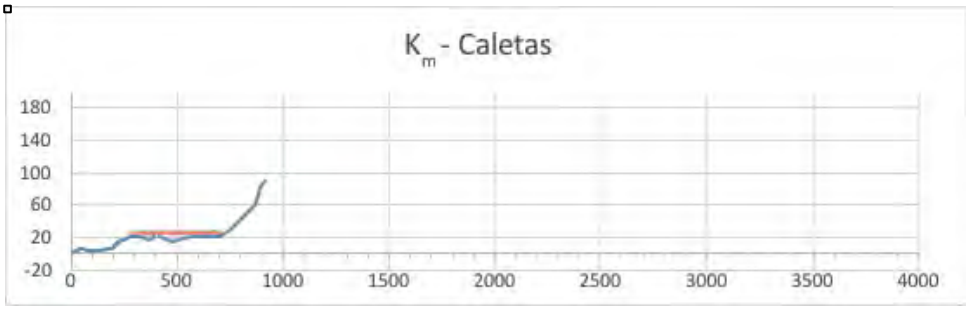

Figure 49: Transect K based on original field data. (Marshall et al., 2010)

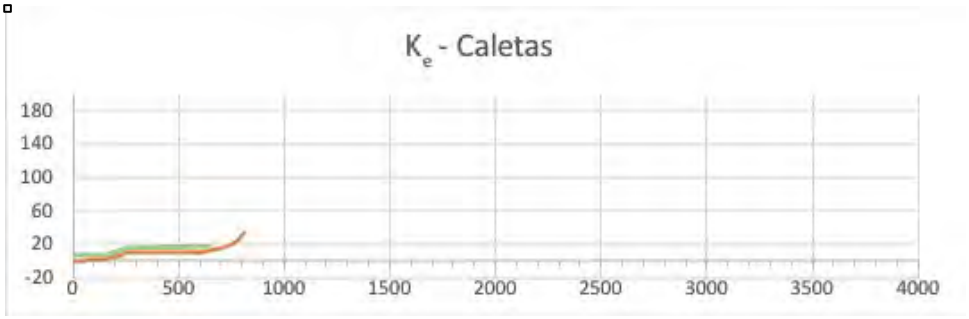

Figure 50: Transect K based on extracted terrace data.

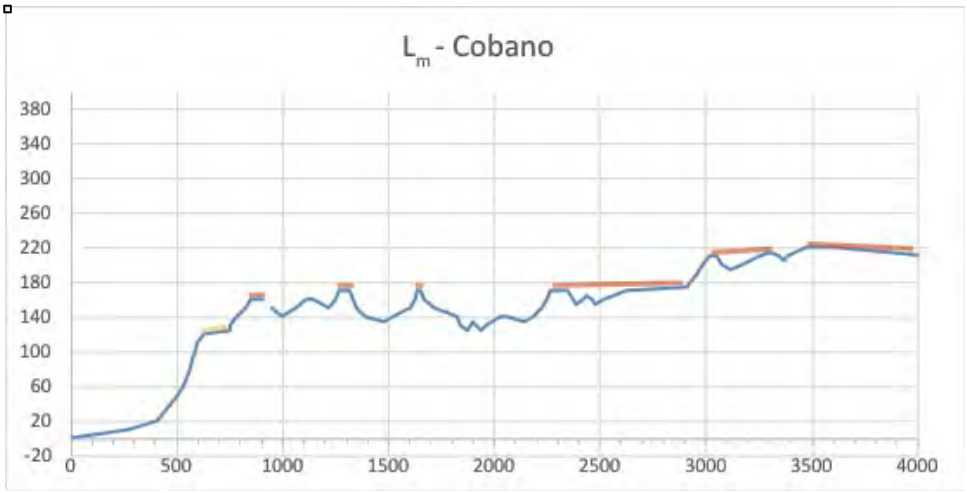

Figure 51: Transect L based on original field data. (Marshall et al., 2010)

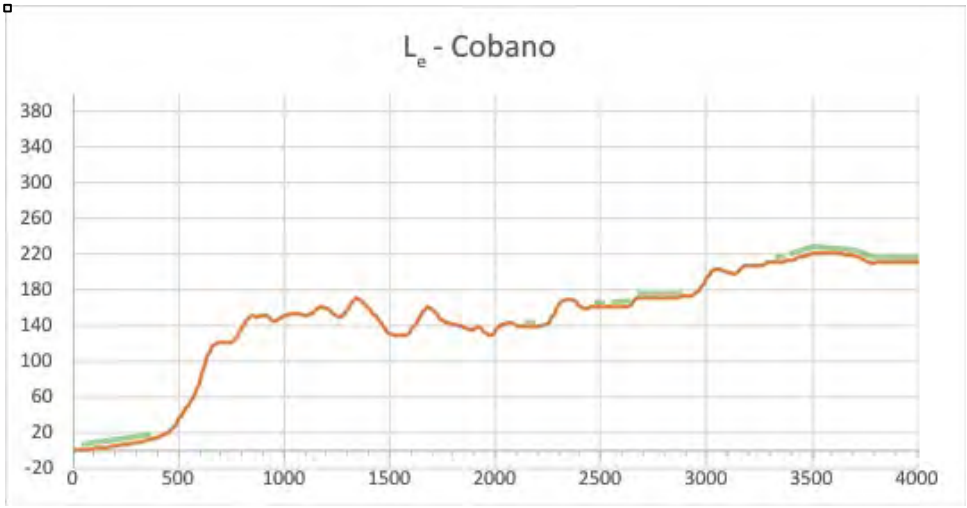

Figure 52: Transect L based on extracted terrace data.

APPENDIX C

ORGINAL FIELD DATA

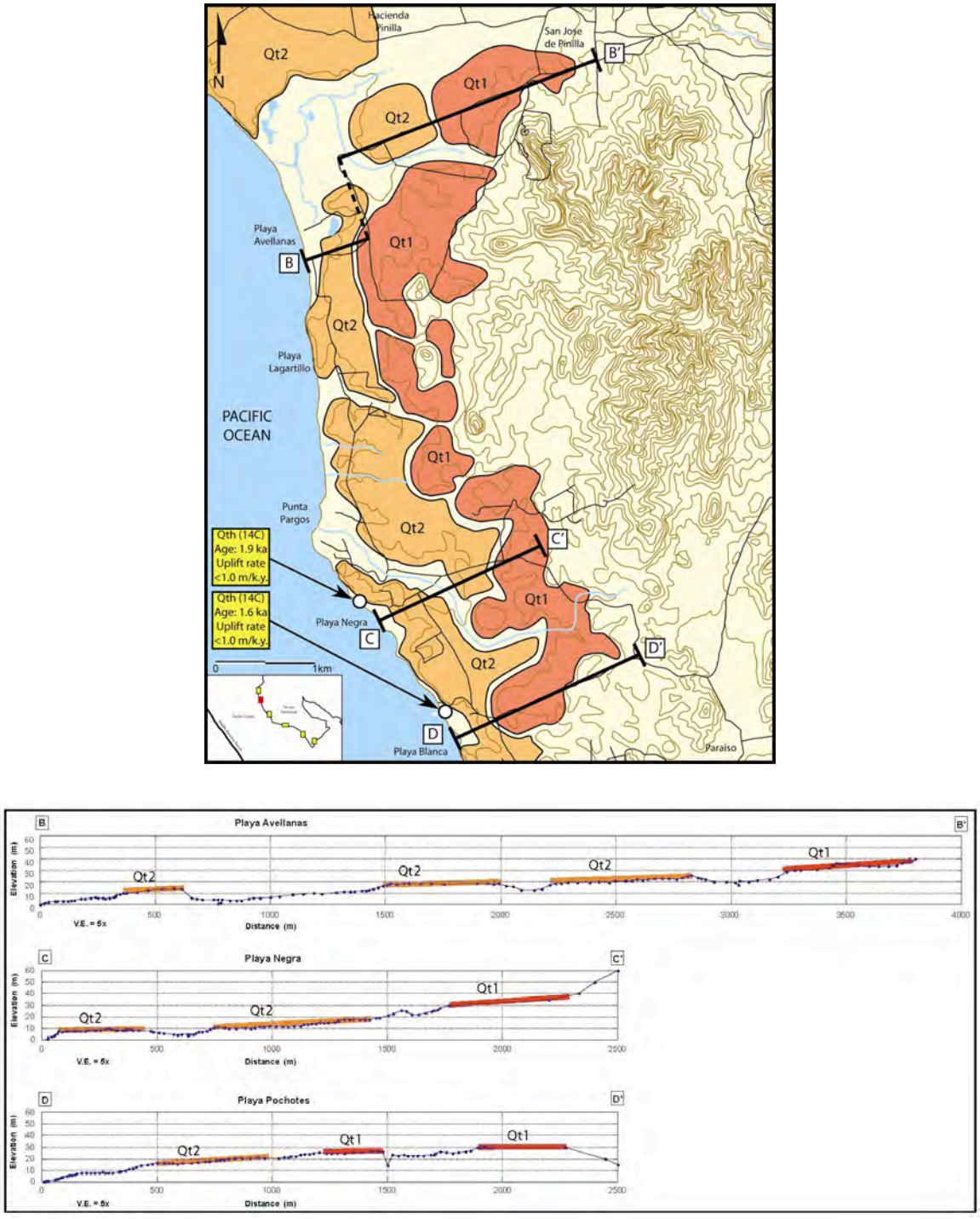

Figure 53: Marine terrace map and surveyed elevation profiles for Field Site #2 [Figure 8] showing locations of Qt1 and Qt2 terraces (Marshall et al., 2008, 2010, 2012).

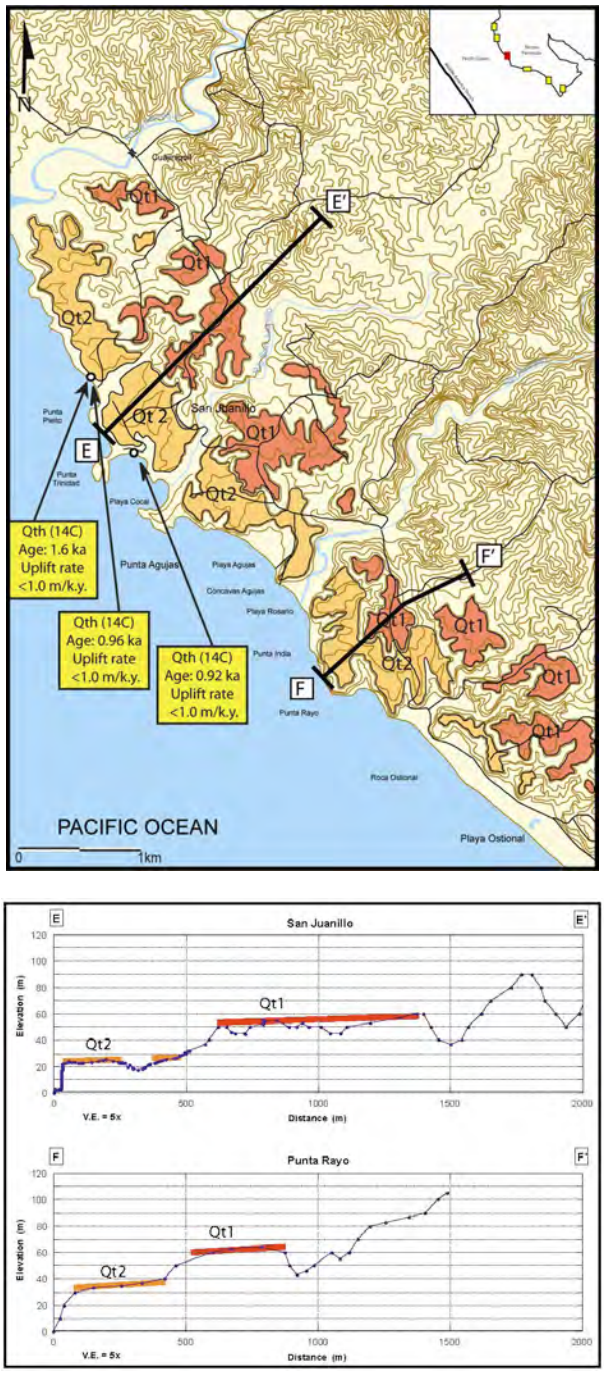

Figure 54: Marine terrace map and surveyed elevation profiles for Field Site #3 [Figure 8] showing locations of Qt1 and Qt2 terraces (Marshall et al., 2008, 2010, 2012)..

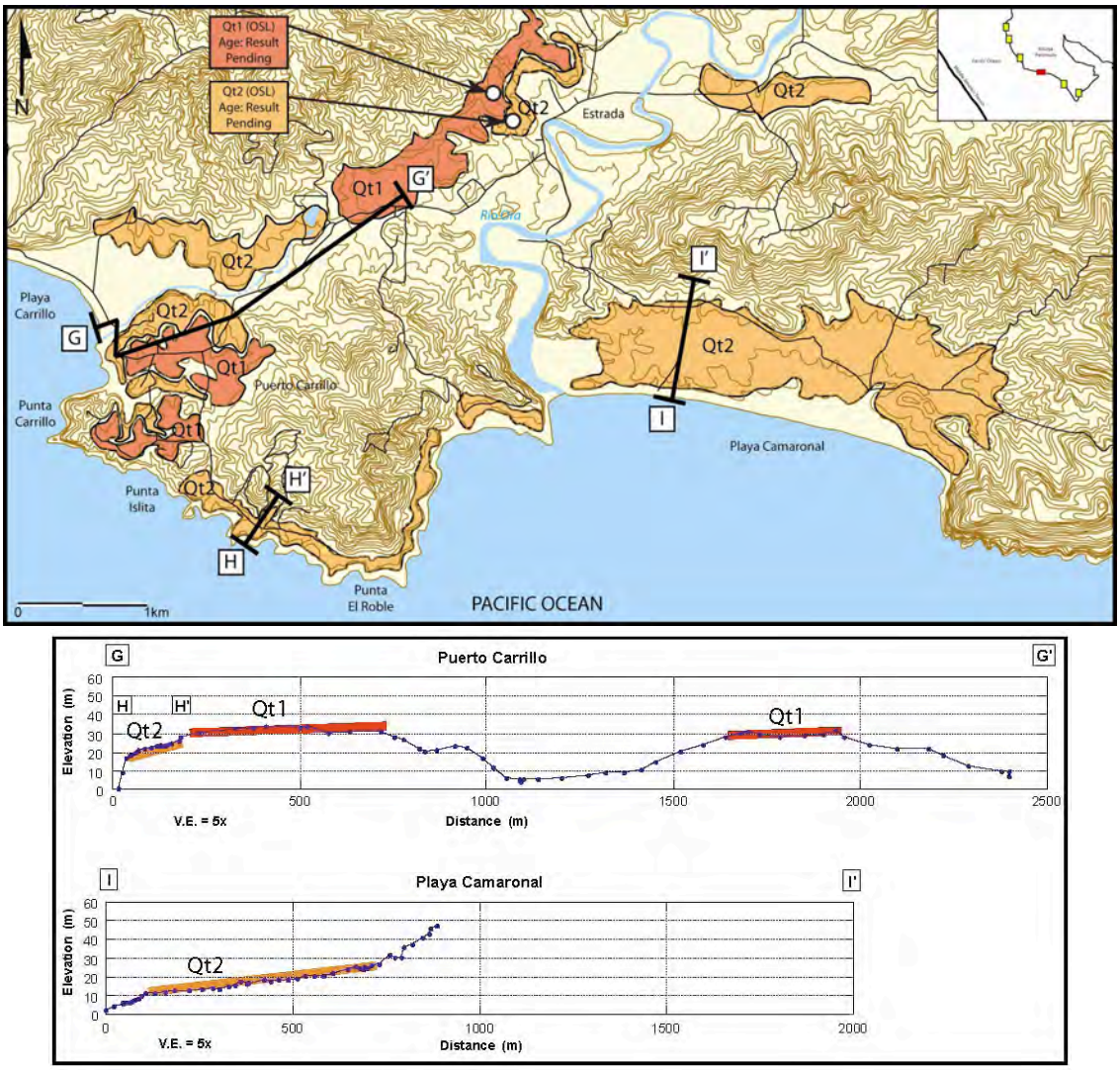

Figure 55: Marine terrace map and surveyed elevation profiles for Field Site #5 [Figure 8] showing locations of Qt1 and Qt2 terraces (Marshall et al., 2008, 2010, 2012).

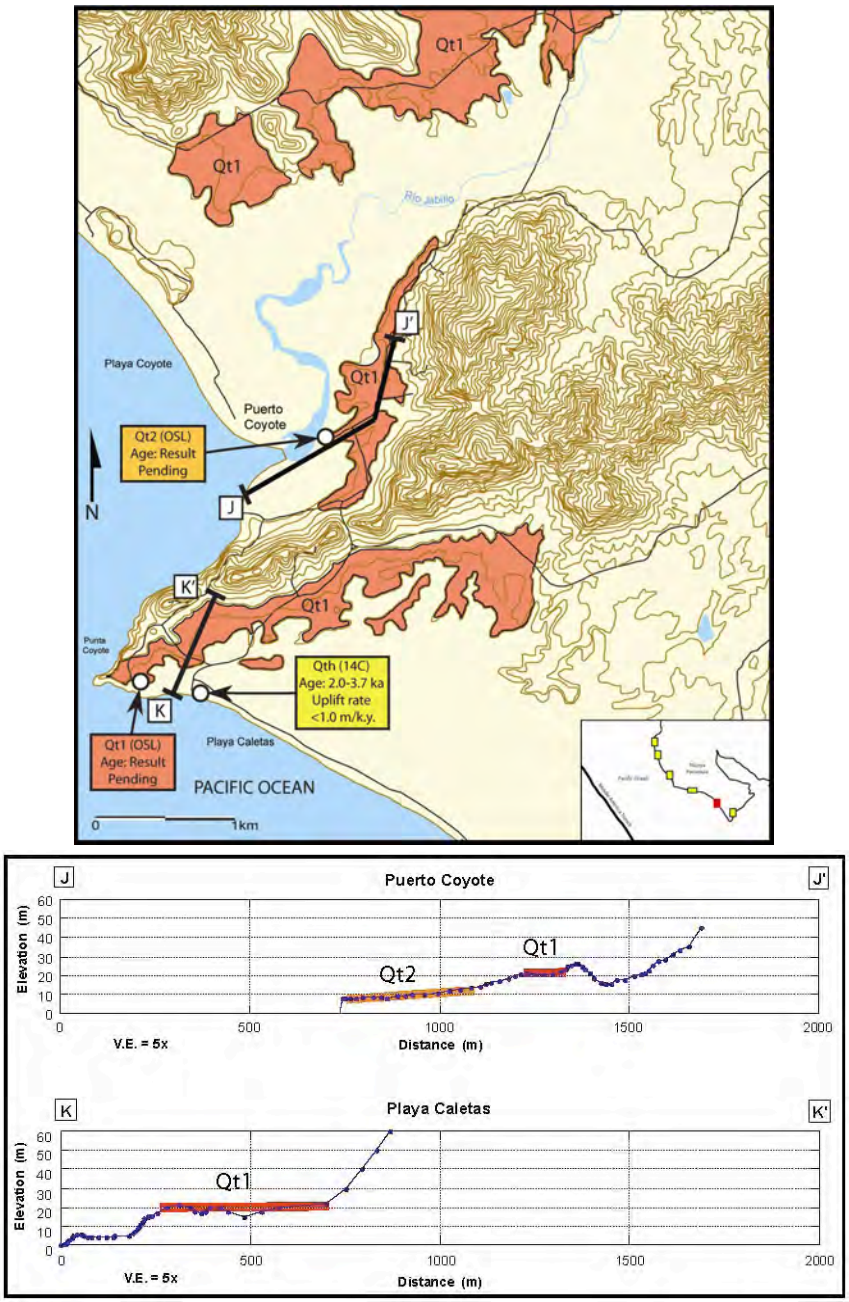

Figure 56: Marine terrace map and surveyed elevation profiles for Field Site #6 [Figure 8] showing locations of Qt1 and Qt2 terraces (Marshall et al., 2008, 2010, 2012).

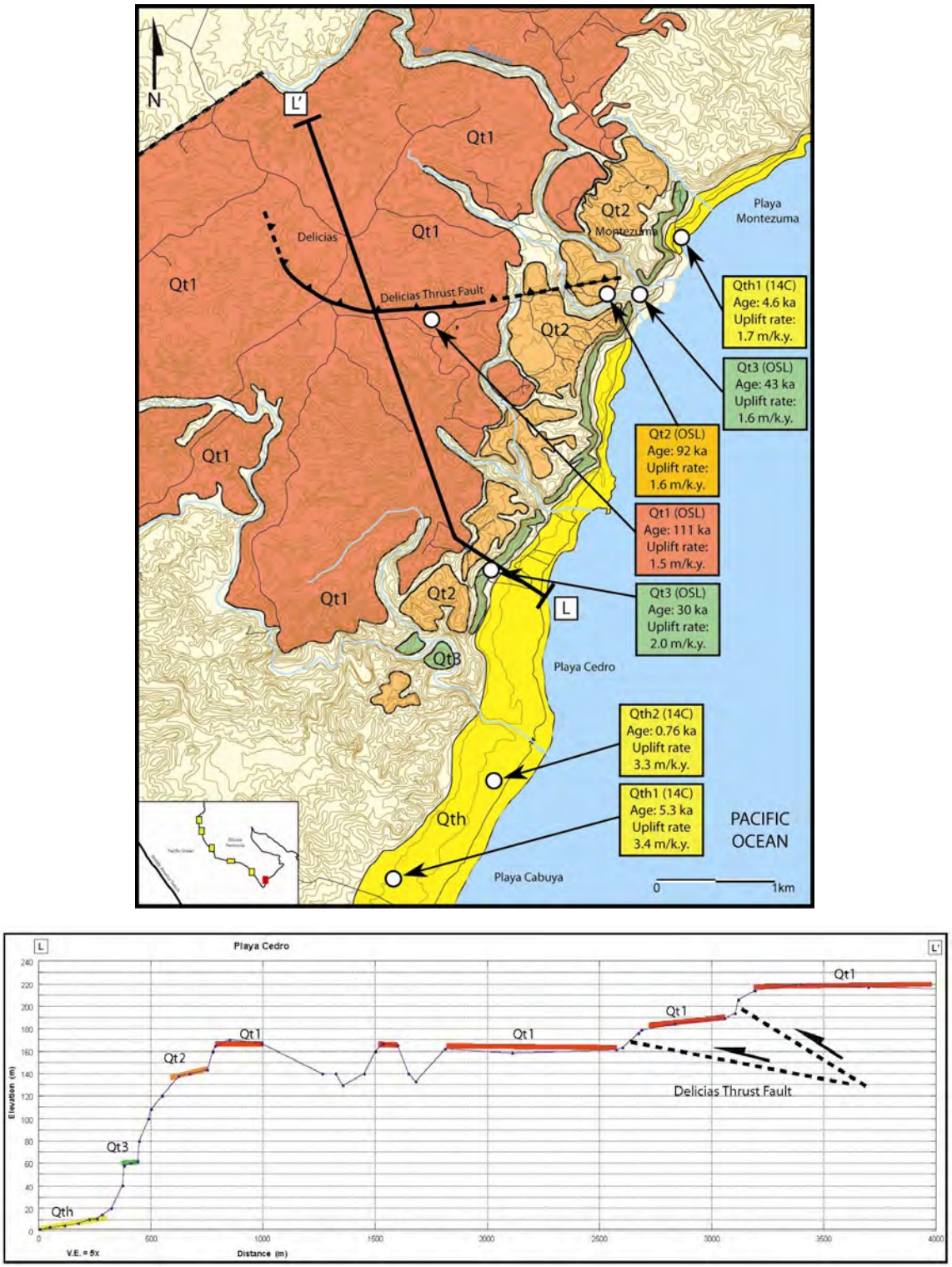

Figure 57: Marine terrace map and surveyed elevation profiles for Field Site #7 [Figure 8] showing locations of Qt1 and Qt2 terraces (Marshall et al., 2008, 2010, 2012).

APPENDIX D

Sea Level Correlation Curves (Marshall et al., 2010)

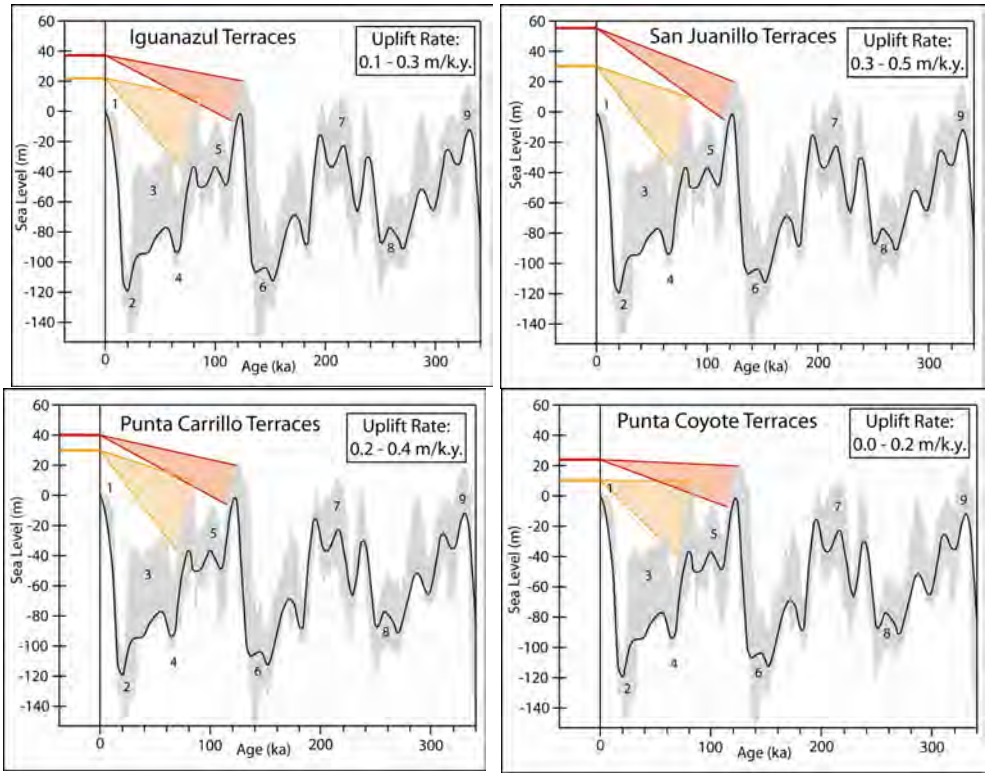

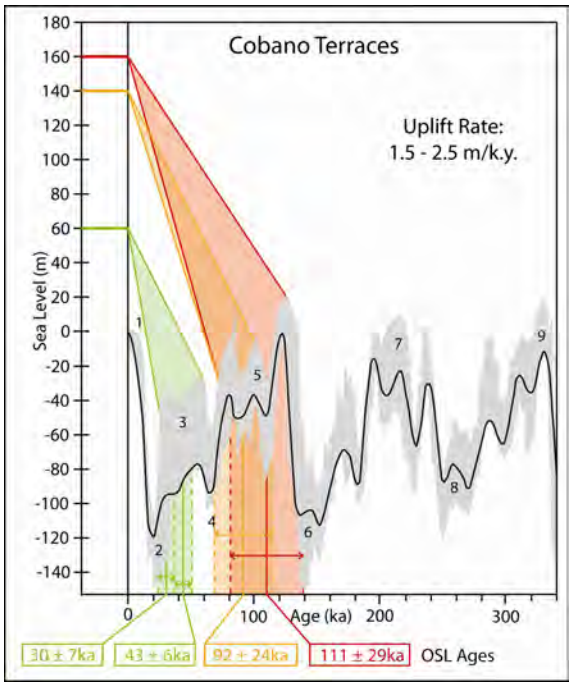

Figure 58: a-f. Sea level correlation diagrams for terrace sequences in each field area (Fig. 49, sites 1-7). Terrace inner edge elevations (at left) are linked to eustatic sea level high stands with colored envelopes that represent a range of possible uplift rates (slope = uplift rate). Correlations are constrained by comparison with OSL dated terraces at Cabo Blanco (Fig. 49, site 7; age data shown on diagram f), and new TCN ages from this study (Fig. 49, sites 2,3,5). Quaternary sea level curve depicts SPECMAP marine oxygen isotope record (solid line; Imbrie et al., 1984), and range of eustatic sea level based on dozens of terrace studies world-wide (grey envelope; Rabineau et al., 2006).